# Ongoing meteor work

## A Comprehensive List of Meteor Showers Obtained from 10 Years of Observations with the IMO Video Meteor Network

*Sirko Molau* [1] *and Jürgen Rendtel* [2]

We have analysed data of more than 450 000 video meteors recorded over more than 10 years in the IMO Video Network. The single station data cover all Solar longitudes and allow to derive positions of radiants and the corresponding velocities as well as activity information for meteor showers. We present results for 9 major showers, 44 minor showers and 12 new detections. Shower data are compared with the entries kept by the IAU Meteor Data Center. For some showers we find a systematic shift of the velocity during the activity period.

Received 2009 August 10

### 1 Introduction

Video meteor observations have significantly increased our knowledge about meteor showers over the recent years. Whereas first observations of amateurs with image-intensified cameras date back to the 1980s, it was the shift towards automated observation that paved the road for the breakthrough of this technique. For over ten years now, video observers from several countries have collected video meteors in the same fashion and created an unprecedended database of more than 450 000 single station video meteors to date. Starting in 2005, automated statistical analysis procedures were developed to extract reliable meteor shower information from the database. First results were presented by Molau (2006 and 2008). Earlier this years, results from the Japanese SonotaCo network were published (SonotaCo, 2009). They represent an independent data set which is analyses based on different analysis algorithms (double-station) and software (UFO* tool set). The results obtained by SonotaCo were in good agreement with our findings, which proved the maturity of our analysis technique and encouraged us to carry out a new analysis. This time, the automated shower extraction was only the first step. The results for each shower were manually checked and refined. Weak shower detections with strong scatter in radiant position or shower velocity were omitted; showers that were artificially split by the analysis software were joined. We compared the detected shower with the compilation of radiants (Jopek, 2009) in the IAU Meteor Data Center (called MDC list hereafter) and recalculated meteor shower parameters (radiant position and drift, activity interval, meteor shower velocity and activity) after rejecting outliers. The result is a comprehensive list of 65 meteor showers obtained from over ten years of observations in the IMO video network.

In this paper we first introduce the IMO Video Meteor Network, which provided the observational basis for this anaylsis. Then we describe the data set and give an outline of the analysis algorithm. We describe the analysis of selected showers in detail to demonstrate what can be achieved with the data. Thereafter, the detected meteor showers are presented and discussed. We start with nine major well-known showers to explore the limits, when their signal is strong enough to stand out of the sporadic background. Next we concentrate on minor showers, which are marked as established in the MDC list. Moving further towards the detection limit, we present minor showers from the MDC list, who have a working status but could be confirmed by our analysis. Next we list a set of new showers that were obtained from the IMO Video Meteor Database. For each shower, we give the interval of activity, radiant position and drift, meteor shower velocity, the maximum video rate (a measure of the meteor shower activity similar to the visual ZHR) as well as an activity profile. We also state, how many single station meteors from the IMO database were attributed to the meteor shower. Finally we report on short-duration showers from the MDC list, which were only detected after we relaxed the minimum meteor shower duration criterion, and finally we present and discuss those showers that are marked as established in the MDC list, but cannot be detected in our database.

In this paper, we leave out results concerning the Antihelion source (except the Taurid branches) as well as sporadic sources (e.g. Apex and Antapex source). These are frequently detected in the video data, but their analysis deserves special care, because they have large radiation areas and stronger scatter in velocity. We also note that there is a complex of radiants in Perseus and Auriga in September/October, which needs special treatment to identify the individual branches. All of these will be subject of aditional analyses presented in the future.

Throughout the paper, we use the MDC numbers and three-letter codes for the showers. For convenience, we also give the shower designations in the respective sections.

### 2 The IMO Video Meteor Network

The continuous monitoring of the night sky by video meteor cameras started with a first station in Aachen (Germany) in March 1999 (Molau, 2001). Other ob-

[1] Abenstalstr. 13b, 84072 Seysdorf, Germany.
Email: sirko@molau.de
[2] Eschenweg 16, 14476 Marquardt, Germany.
Email: jrendtel@aip.de

IMO bibcode WGN-374-molau-videoshowers
NASA-ADS bibcode 2009JIMO...37...98M

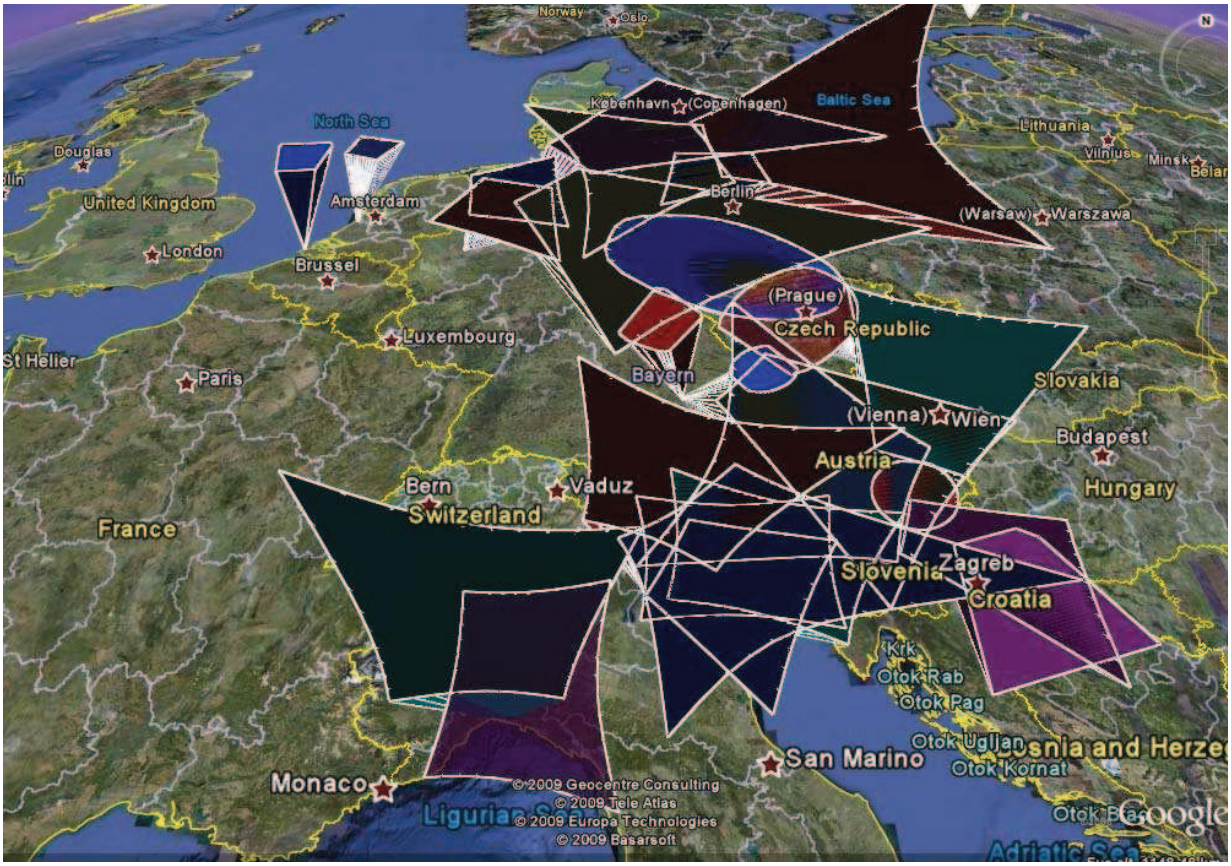


*Figure 1* – Fields of view of the IMO network cameras in Central Europe as of December 2008.

servers joined the AKM network (Arbeitskreis Meteore, AKM), and by the end of 1999, five German observers had collected over 8 000 meteors within 1 000 hours of effective observing time. In the following years, the network grew steadily, and by 2004 it was renamed to IMO Video Meteor Network because of its international character.

The common characteristic of all observers in the IMO network is the use of the MetRec software (Molau, 1998). The PAL/NTSC signal of the video camera is directly fed into the analysis PC, digitized with a Matrox Meteor II framegrabber, and inspected by the MetRec software in real-time. Once a meteor is detected, astrometric and photometric routines are applied. The position, brightness and velocity of each meteor are stored together with a sum image and a short time-sequence of the event. All observers send their data on a monthly basis to the IMO video commission, where they are quality-checked, corrected if necessary, analyzed, archived and published.

Right from the start, the IMO Network focused on single station observation. The major advantage is, that each observer with the right equipment can participate in the network and provide useful data, no matter how many cameras there are in his part of the world. There is no need to synchronize the fields of view and technical parameters of individual cameras for double station work. Each meteor contributes to the analysis independently where and when it was observed, whether there are other recordings from the same event or how the observing geometry looks like. On the other hand, meteor trajectories and orbits cannot be determined directly from single station data. It requires large data sets and sophisticated statistical algorithms to reveal not only the radiant position of meteor showers, but also their pre-atmospheric entry velocity, the interval of activity and activity profiles with high precision.

Two types of video cameras are most popular these days. On the one hand, there are non-intensified Mintron and Watec cameras with Sony ExView HAD chip as sensor, typically equipped with $f/0.8$ Computar c-mount lenses of 3.8, 6, or 8 mm focal length. Their field of view ranges between 40 and 80° with limiting magnitudes between +3 and +4 mag. On the other hand, there are a few image-intensified cameras. Most popular is the Philips XX-1332 second generation image intensifier tube (or other brands of the same device) with 50 mm photo cathode. In connection with a $f = 50$ mm $f/1.4$ standard photographic lens, it achieves a field of view of roughly 60° at limiting magnitudes beyond +6 mag. Under dark skies, image-intensified cameras record on average about a factor of three more meteors than non-intensified cameras, but they are more delicate and therefore difficult to handle in automated systems.

Over the years, the degree of automation has increased significantly in the IMO network. In the beginning, the cameras were manually started in clear nights. Nowadays, most cameras are operated fully automated. They are activated by a time switch in the evening and

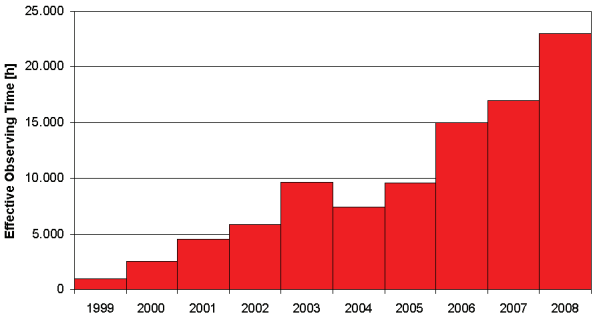


*Figure 2* – Effective observing time of the IMO Video Meteor Network 1999–2008.

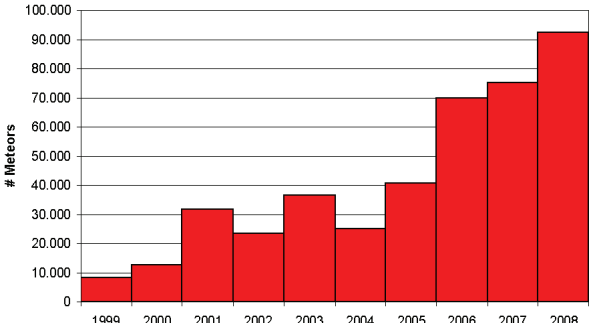


*Figure 3* – Number of meteors recorded by the IMO Video Meteor Network 1999–2008.

shut down automatically in the morning. Thus, they cover meteor activity at any time with clear skies. Also the size of the network has extended significantly over the last ten years. Most parts of Central Europe are well covered (Figure 1), and two cameras are operated in North America.

Thanks to the network size and the high degree of automation, the amount of data and their quality have increased significantly over the recent years. In 2008, 24 observers from ten countries contributed to the network with overall 37 cameras (Molau & Kac, 2009). They recorded more than ten times as many meteors within twenty times as many observing hours than in 1999. Between 2006 and 2008, there was just a single night without a meteor record because of poor weather at all sites. Figure 2 shows the total effective observing time in the IMO Video Meteor Network, and Figure 3 the number of meteors recorded each year. Until mid-2009, more than 30 observers from twelve countries (Australia, Czech Republic, Finland, Germany, Hungary, Italy, Portugal, Slovenia, Spain, the Netherlands, UK, and the USA) submitted their data.

## 3 Data set and analysis procedure

The analysis presented here is based on all data collected by the IMO network until June 2009. Thus, beside the main data set 1999–2008, also roughly 5 000 meteors recorded before the start of the network (1993–1998) and 31 000 meteors from the first half of 2009 were included. The resulting data set consists of 451 282 single station meteors recorded in 3 363 observing nights and 107 594 hours of effective observing time. Table 1

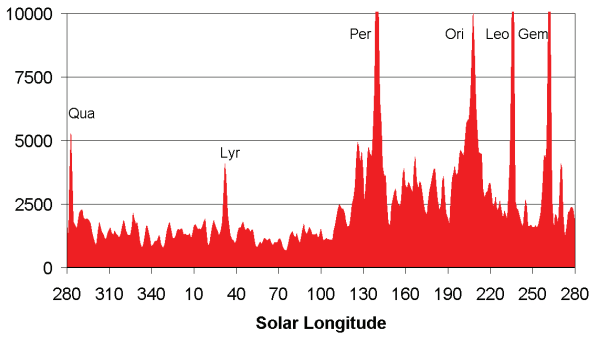


*Figure 4* – Distribution of meteors over Solar longitude. Due to overlapping sliding intervals, each meteor contributes twice.

gives an overview of all observers contributing more than ten observing nights to the video database. We are grateful to their passion, which enabled the collection of this to-date unprecedented data set of high-quality meteor recordings in the optical domain, completely covering all solar longitudes.

Figure 4 depicts the distribution of meteors over Solar longitude. The analysis was based on sliding intervals of two degrees length and one degree shift, so each meteor contributed to two consecutive solar longitude intervals. The times of the major showers with up to 16 000 meteors per interval are clearly visible. But also times of low meteor shower activity are well covered – there is no single interval with less than 680 meteor records. The average is close to 2 500 meteors per interval.

The procedure used to analyze this data set has been applied first to a smaller subset in 2006 (Molau, 2006). It was refined in a second analysis (Molau, 2008). Here we give a short summary of the algorithms.

For each meteor, the time and place of observation as well as the coordinates of the start and end point and the angular velocity are given. Meteor shower radiants are described by four parameters: their position (right ascension $\alpha$ and declination $\delta$), velocity at infinity $V_\infty$, and the Solar longitude $\lambda_\odot$. For each pair of meteor $m$ and radiant $r$, a conditional probability $P(m|r)$ can be calculated. It describes the probability, that the meteor belongs to the (zenith attraction corrected) radiant. The conditional probability is computed from two measures – the distance $d$ (in °) at which the backward prolongation of the meteor misses the radiant, and the difference $v$ (in °/s) between the expected and the observed angular meteor velocity. The expected angular velocity that a meteor from radiant $r$ would have at the position of $m$, is calculated on the basis of the average meteor altitude, which was recently refined (Molau & SonotaCo, 2009). Both the radiant miss distance and the angular velocity difference are combined in a three-dimensional Laplacian probability distribution. The type of distribution and its parameters were obtained from data (Molau, 2008) and reflect typical video observation errors:

*Table 1* – Observers who contributed more than 10 observing nights to the IMO Video Meteor Network.

| Observer | Country | IMO Code | Nights | Eff. obs. time [h] | Meteors |
|---|---|---|---|---|---|
| Sirko Molau | DE | MOLSI | 2344 | 20 807.2 | 127 072 |
| Jörg Strunk | DE | STRJO | 1696 | 12 709.4 | 42 009 |
| Javor Kac | SL | KACJA | 1173 | 10 333.0 | 31 354 |
| Ilkka Yrjölä | FI | YRJIL | 942 | 5 419.2 | 18 596 |
| Stane Slavec | SL | SLAST | 871 | 4 318.9 | 11 262 |
| Flavio Castellani | IT | CASFL | 794 | 5 775.4 | 13 802 |
| Orlando Benitez-Sanchez | ES | BENOR | 733 | 4 088.3 | 10 473 |
| Jürgen Rendtel | DE | RENJU | 647 | 3 823.4 | 17 223 |
| Bernd Brinkmann | DE | BRIBE | 598 | 2 376.2 | 8 366 |
| Detlef Koschny | NL | KOSDE | 509 | 3 126.3 | 11 567 |
| Mihaela Triglav | SL | TRIMI | 505 | 2 585.9 | 8 474 |
| Robert Lunsford | US | LUNRO | 495 | 3 204.2 | 22 122 |
| Enrico Stomeo | IT | STOEN | 492 | 3 605.5 | 13 854 |
| Stephen Evans | UK | EVAST | 457 | 2 807.3 | 11 411 |
| Wolfgang Hinz | DE | HINWO | 455 | 2 689.5 | 13 690 |
| Carl Hergenrother | US | HERCA | 399 | 2 805.7 | 5 570 |
| Steve Quirk | AU | QUIST | 341 | 3 041.8 | 10 109 |
| Rui Goncalves | PT | GONRU | 320 | 2 850.6 | 9 931 |
| Stefano Crivello | IT | CRIST | 229 | 1 459.4 | 6 217 |
| Biondani Roberto | IT | ROBBI | 229 | 1 261.6 | 4 082 |
| Mirko Nitschke | DE | NITMI | 213 | 942.5 | 5 425 |
| David Przewozny | DE | PRZDA | 196 | 1 073.6 | 3 745 |
| Stefan Ueberschaer | DE | UEBST | 173 | 882.3 | 1 684 |
| Maurizio Eltri | IT | ELTMA | 169 | 1 210.4 | 5 886 |
| Ulrich Sperberg | DE | SPEUL | 159 | 1 021.6 | 4 339 |
| Paolo Ochner | IT | OCHPA | 134 | 733.2 | 1 763 |
| Rosta Stork | CZ | STORO | 98 | 1 052.8 | 14 732 |
| Rob McNaught | AU | MCNRO | 52 | 401.2 | 5 285 |
| Andre Knöfel | DE | KNOAN | 47 | 289.0 | 648 |
| Klaas Jobse | NL | JOBKL | 47 | 288.0 | 2 231 |
| Mitja Govedič | SL | GOVMI | 33 | 156.7 | 489 |
| Antal Igaz | HU | IGAAN | 32 | 217.7 | 369 |
| Miloš Weber | CZ | WEBMI | 29 | 49.4 | 1 050 |
| other | | | 25 | 186.8 | 6 452 |
| Overall | | | 3363 | 107 594.0 | 451 282 |

$$P(m|r) = \exp(-0.8 \times d) \times \exp\left(\frac{-v}{0.4 + v/50}\right).$$

Based on the conditional probability, a search for possible meteor shower radiants is carried out, which is the computationally most demanding part of the analysis. At first the data set is cut into Solar longitude slices (two degrees length, one degree shift). For each Solar longitude interval, an iterative search procedure is carried out.

At initialization, the probability of each possible radiant point (position in steps of $0.^\circ5$, velocity at infinitiy in steps of 1 km/s) is accumulated over all meteors of the interval. The probability distributions of individual meteors are not normalized, i.e. the most probable radiant gets a value of 1.0 and the probability mass provided by each meteor differs. In the iterative phase, the radiant with highest accumulated probability is selected. According to standard criteria for meteor shower assignment, all meteors belonging to that radiant are determined and taken out of the data set. Their probability distribution is calculated and subtracted from the overall distribution. Then the next iteration is carried out to extract the next strongest radiant. The procedure terminates after 50 iterations. To avoid interference of nearby radiants, the meteor shower assignment is repeated once all radiants are determined (Molau, 2008).

After the most probable radiants are determined for each solar longitude, similar radiants in consecutive Solar longitude intervals are connected to identify meteor showers. The showers are compared against the current MDC list (Jopek, 2009) to classify known showers. The main parameters that determine the number and quality of detected meteors showers are the minimum number of intervals with suitable radiants (minimum meteor shower duration: 5° in Solar longitude), the maximum position difference (7°) and the maximum velocity difference (7 km/s) between the radiants from one Solar longitude interval to the next. In brackets are the figures use primarily for this analysis.

Once the meteor showers were determined, their basic parameters (activity interval and date of maximum activity, radiant position and drift, average velocity) were calculated. To compute the meteor shower activity is in particular challenging, as the data set was a mixture of observations from different cameras with different lenses under different observing conditions. Neither the effective observing time nor the field of view nor limiting magnitude per Solar longitude were known. At first, the observation probability (Molau, 2008) was applied to each meteor that belongs to a detected radiant. This probability is the average of the sine of the radiant altitude at night time in the given solar longitude interval. A meteor from a hypothetical radiant that is all night long at zenith would get a weight of 1.0, whereas a meteor from a radiant that is visible for only a short time near the horizon would get a weight of up to 100. This way, the geometric observing conditions are corrected – typical observability function weights at mid-northern latitude range between 1.5 for easily visible Geminids and 30 for the difficult to observe $\eta$-Aquariids.

In the next step, all meteors that belong to showers are counted, and all remaining meteors are declared as sporadics. The meteor shower activity (called video rate VR hereafter) at a certain Solar longitude is now the ratio between the observability function corrected number of shower meteors and the number of sporadics in that interval. This way, the difference in effective observing time, field of view diameter and limiting magnitude is accounted for.

Finally, the video rate is scaled and corrected for the annual sporadic activity variation. It was found that the sporadic activity in the Northern hemisphere can be approximated by a sine shaped function with a minimum of 2.2 meteors per hour at Solar longitude 350° and a maximum of 4.2 at 170° (Molau, 2008). The scaling factor was initally chosen such that the $\eta$-Aquariids yield a maximum VR of 50. It turned out, that the video rate VR resembles the long-term ZHR of a shower remarkably well. Thus, we are confident that we can not only give a qualitative account of meteor shower activity (shape of the activity profile and time of the maximum), but also a quantitative estimate of the ZHR. Due to the 2-day-intervals, however, the peaks are significantly smoothed out and therefore below the peak ZHRs derived from short intervals.

## 4 Manual refinement

All automatically detected showers were manually checked. When the video rate of a shower falls below one, the sporadic dilution becomes dominating. For this reason, there are typically a few uncertain intervals at the begin and end of each shower activity period, which are affected by chance alignments with sporadic meteors. We reduced the activity intervals of each shower to those with radiant position and velocity fitting well to the average shower parameters. We corrected cases, where one shower was cut into two, and we omitted showers, which contained only few meteors and showed strong scatter from one solar longitude interval to the next.

To account for meteor showers of shorter duration, we repeated the meteor shower search with reduced minimum meteor shower duration of four and three degrees in Solar longitude. Naturally, the number of possible showers grew significantly, so we focused on those which were not found in the previous analysis with longer duration, and which fitted well to showers from the MDC list.

In the next steps, the meteor shower parameters were refined. The position and drift of the radiant was re-calculated in the possibly reduced Solar longitude interval by a weighted linear regression, with the absolute meteor counts per interval taken as weight. For major showers, the Solar longitude of the maximum activity was re-calculated as the weighted mean Solar longitude, using only the intervals of highest activity with the video rate as weight. The meteor shower velocity was refined as well. It is the average over all Solar

longitude intervals. Here, each value was weighted by the meteor number. This allows us to report both the Solar longitude (i.e. date) of the shower maximum and the velocity rounded to the nearest 0.1 degree or km/s, respectively, even though the underlying analysis was carried out for steps of 1 degree in solar longitude and 1 km/s in velocity $V_\infty$.

We estimate that the accuracy of the radiant position is better than 1° if the activity VR $\geq 2$, and the average velocity at infinity is accurate to 1 km/s for all showers.

## 5 Meteor shower velocities

When calculating the radiant position and drift for long duration meteor showers, we noted that in some cases the meteor shower velocity did not only show some arbitrary scatter around the average value, but that the calculated velocity increased or decreased systematically over the activity period. At first we did not pay special attention to this observation, because we assumed that to be an artefact of the analysis procedure. However, on our request, the Japanese meteor observer SonotaCo checked his data set of meteoroid orbits obtained from the SonotaCo video network (SonotaCo, 2009) and found similar variations. Even more, for all four showers which have been compared in detail (ETA, PER, SDA and ORI), he reported exactly the same behaviour (decreasing, constant or increasig velocity) with only little deviation in the amount of the velocity change.

As both data sets and analysis procedures are completely independent, we conclude that the observed variations in meteor shower velocity over time are real. For this reason, we add the detected variation in velocity (in km/s per degree in Solar longitude) for all major and long-lasting showers with sufficient data. We found that LYR, ETA, and KCG are showers with a particularly large increase in velocity over time, whereas SDA, QUA, CAP, NOO and JPE show considerable velocity decreases.

As the Earth crosses different sections of the meteoroid stream over a longer period which have undergone numerous and variable orbit perturbations, these variations need to be correlated with the Earth-meteoroid collision geometry. For example, we find that the shift is in the opposite direction for the Orionids and the $\eta$-Aquariids, and larger in the latter case. As the showers represent different cross-sections through the same meteoroid stream with the Orionids being the far more distant path from the centre, the numbers listed in Table 2 indicate that this effect may also be related to different ejection speeds from the parent comet. However, at this time we have no proven explanation for the observed velocity changes.

## 6 Application of the method and results of radiant searches

First of all, our data provides us with a detailed set of information about all major showers, such as their activity period and their radiant position and drift. The

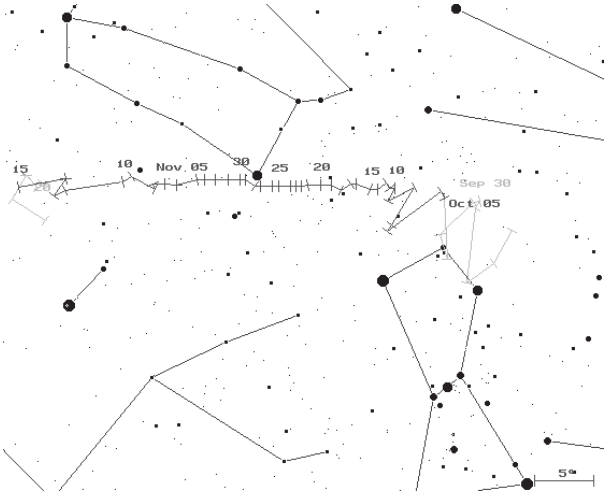


*Figure 5* – Radiant of the Orionids derived from the video data. The shaded (grey) parts at the outer edges of the drift path show the position found from the data which were excluded because of the position uncertainties.

MDC list distinguishes between showers that are established and those which have a working list status, labelled 'e' and 'w', respectively. The Toroidal, Apex and Antihelion sources also occur in our data set. In this paper, we concentrate on showers which are linked to neither of these permanent sporadic and ecliptical soures (except the Northern and Southern Taurids), because the analysis method was adjusted for showers with compact radiants. Sources with diffuse radiation areas would need to be treated in a different way in an extra paper. Another complex which we found deserves a detailed separate analysis is the set of showers radiating from the Perseus-Auriga region from end-August to mid-October. Of these showers, we only list the Aurigids and the September $\varepsilon$-Perseids here.

### 6.1 Major showers

The nine meteor showers with the highest activity level have been used for testing and calibrating the detectability of radiants from the data sample. We present details for the Orionids and the Quadrantids, because our results extend beyond the confirmation of their radiant position and drift and their activity level. In both cases, our data indicate a longer period in which the activity and the radiant can be clearly detected. Our activity profiles are from data collected over about a decade and for the search algorithm we also bin over an interval length of 2° in Solar longitude. For these reasons, our profiles are smoother than the graphs calculated from short binning intervals, and the peak level of the VR remains well below the peak ZHRs listed for the showers.

The **Orionids** can be observed from both hemispheres. The date of the peak as well as the radiant position and drift found from our data agree perfectly with the data stored in the MDC list. When we look at the outer edges of the shower activity, we find that the radiant can be continuously followed towards earlier and later Solar longitudes (Figure 5). Both the video

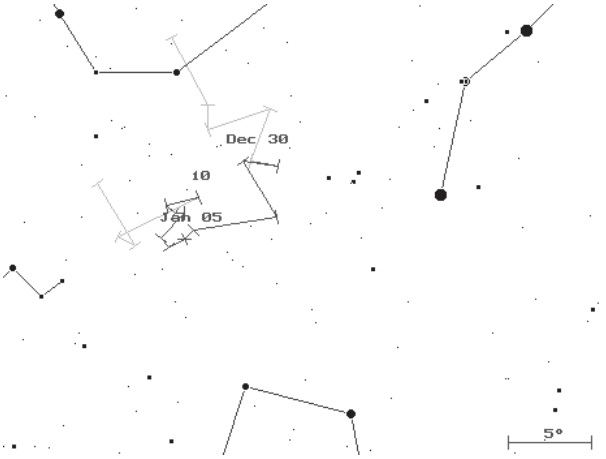


*Figure 6* – Radiant of the Quadrantids derived from the video data. In this case the position becomes uncertain in the outer bins.

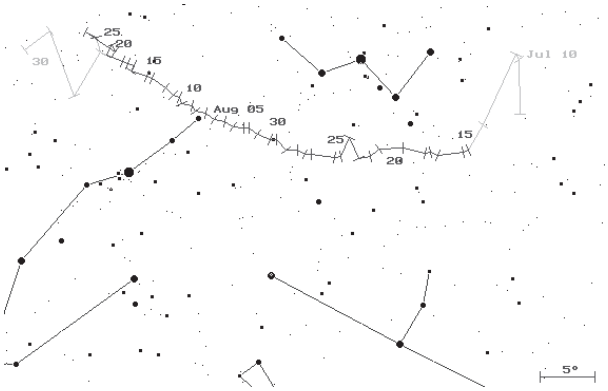


*Figure 7* – Radiant of the Perseids derived from the video data. Towards the ends, the radiant position becomes unreliable.

rate VR (shown in Figure 8) and the steady shift of the radiant position in combination with the same velocity of the meteoroids leads to an activity period which extends from end-September to November. Both parameters limit the detectability of the activity from a radiant.

Our video *rate calibration* is based on the $\eta$-Aquariids. The comparison between the VR and the long-term ZHR allows us to set a detection limit of VR = 0.7. The other limit is the reliability of the radiant position. The lower the number of true shower meteors is, the larger is the amount of sporadic meteors accidentially lining up with the radiant (and fitting the velocity). As a result of the sporadic effect, the calculated position will become uncertain and the radiant deviates from the position calculated for the neighbouring bin as shown for the Orionids in Figure 5. If these differences exceed 3° in neighbouring bins, we do not regard this as the signal of a detectable shower. These limits have been generally applied to all detections later. **Conclusion:** the detection of showers from the current data sample is possible if VR $\geq$ 0.7 and $(\Delta\alpha, \Delta\delta) \leq 3°$ per 1° in Solar longitude.

The **Quadrantids** show peak rates which are among the strongest of all showers currently observable from the Earth. Usually, the shower activity is assumed to start on January 1 and to cease by January 6. Again, our analysis shows a perfect agreement in the complete data set for the near-peak period. Moreover, the activity obviously extends in both directions. We detect meteors from the region associated to the Quadrantids from $\lambda_\odot$=274° (December 27) to 292° (January 12) with VR $>$ 0.9 all the time. As shown in Figure 6, the recorded meteors do not define a reliable radiant before 281° and after 290°. Hence we give the Quadrantid activity period as $\lambda_\odot = 281° - 290°$, here limited by the consistency of the radiant drift, although the *averaged drift* after 290° is still consistent with the period before this date. Whether the radiant becomes diffuse or this is just an effect of the small sample, cannot be decided from our analysis method.

The complete list of data obtained from the most active showers are summarized in Table 2 and compared with the MDC list entries. Graphs representing the activity in terms of VR are shown in Figure 8.

**6 LYR (Lyrids):** we find VR $\geq$ 0.6 for the entire period 24–36°; the radiant drift becomes inconsistent only in the first and last bins – hence the period of detectability is limited to 26–35°. In this interval, the VR is $\geq$ 0.7 (Figure 8).

**31 ETA ($\eta$-Aquariids):** the relative rate is VR $\geq$ 4.0 between 36 and 61°. Rather few ETA meteors have been recorded after May 18 (57°) obviously due to the shorter observing window at most observing locations. Hence the radiant position starts to become inconsistent particularly after $\lambda_\odot = 61°$ while it gives a smooth drift for the entire period before this date. Our data defines the shower over the interval $38 - 60°$. The peak rate was earlier used for calibrating the VR, hence, consistently, we find a maximum VR $\approx$ 54 (Figure 8). The velocity shift of 0.12 km/s per 1° in Solar longitude over the cross-section of the stream has been discussed in Section 5. The shift during the ETA activity is larger than in the Orionid period. The ETA meteoroids are closer to the parent's orbit and thus perhaps represent a larger variation in the ejection conditions from the inner to the outer regions of the stream.

**7 PER (Perseids):** we find VR $>$ 4 even towards August 30, but the radiant position calculated from the video data varies after August 26 (Figure 7). From the radiant data, we can trace the shower over the period 110–153° (July 13–August 26). In this case the variations of the derived radiant position in consecutive bins exceed the threshold set for a reliable shower identification while the VR would be still well above the limit. The large number of Perseids essentially in all bins also causes additional detections in the vicinity of the Perseid radiant fitting velocity and radiant drifts similar to that of the major shower. In all these cases, these virtual radiants show very large scatter in their coordinates from one bin to the next (typically more than 3°) being not parallel to the ecliptic, indicating that these are artefacts. Similar effects need to be carefully checked if detections during other major showers occur.

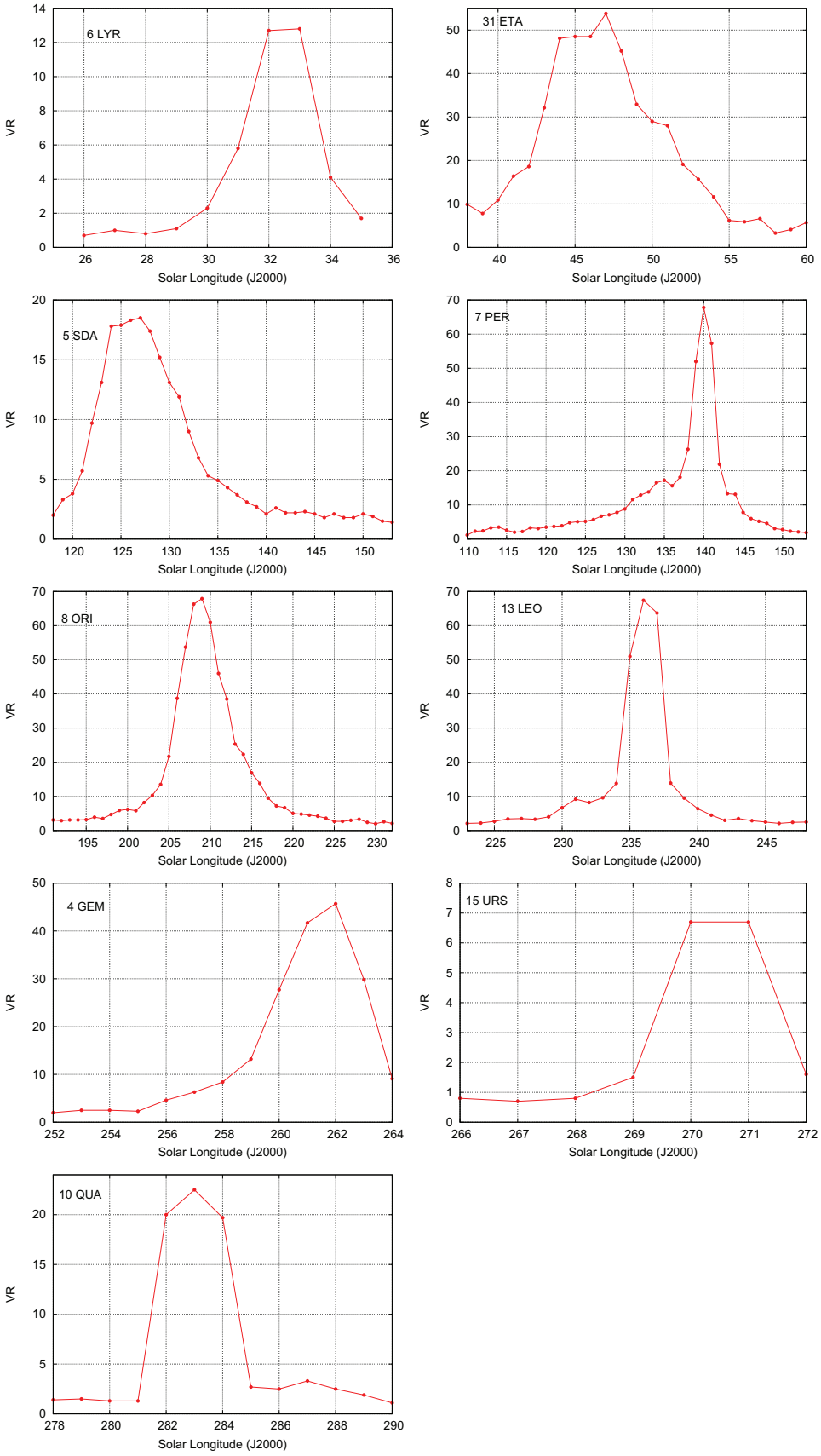


*Figure 8* – Activity profiles for the major showers derived from our video data sorted by the Solar longitude of their occurrence (same as in Table 2).

*Table 2* – Data of the major meteor showers sorted by Solar longitude (J2000.0). (V) refers to the obtained video data, (L) gives the values of the MDC list. $\Delta V_\infty$ is the observed average velocity drift over the activity period in km/s per 1° in Solar longitude. Data Met. is the number of meteors from the shower in the video database

| Shower | Peak $\lambda_\odot$[°] | | Period $\lambda_\odot$[°] | | Radiant position and drift [°] | | | | $V_\infty$ [km/s] and $\Delta V_\infty$ | | | Max. | Data |
|---|---|---|---|---|---|---|---|---|---|---|---|---|---|
| | (V) | (L) | (V) | (L) | $\alpha$ | $\Delta\alpha$ | $\delta$ | $\Delta\delta$ | (V) | | (L) | VR | Met. |
| 6 LYR | 32.4 | 32 | 26– 35 | 26– 35 | 272.2 | +0.57 | +32.9 | −0.43 | 46.2 | +0.18 | 48.4 | 13 | 1516 |
| 31 ETA | 46.8 | 46 | 38– 60 | 29– 67 | 338.9 | +0.67 | − 0.6 | +0.32 | 66.8 | +0.12 | 66.9 | 54 | 1051 |
| 5 SDA | 126.9 | 125 | 118–150 | 110–146 | 340.4 | +0.86 | −16.4 | +0.28 | 43.6 | −0.26 | 42.0 | 19 | 4716 |
| 7 PER | 140.0 | 140 | 111–153 | 114–151 | 48.1 | +1.44 | +57.6 | +0.25 | 59.0 | 0 | 60.5 | 68 | 22169 |
| 8 ORI | 208.9 | 208 | 191–232 | 189–224 | 96.1 | +0.78 | +15.5 | +0.03 | 67.3 | −0.06 | 67.1 | 68 | 18249 |
| 13 LEO | 236.1 | 235 | 223–248 | 227–241 | 154.2 | +0.61 | +21.6 | −0.29 | 70.6 | 0 | 71.5 | 67 | 9874 |
| 4 GEM | 261.5 | 262 | 252–265 | 255–265 | 113.3 | +0.96 | +32.2 | −0.17 | 35.0 | 0 | 36.4 | 46 | 13193 |
| 15 URS | 270.5 | 271 | 266–272 | 265–274 | 217.6 | +1.60 | +74.8 | −0.13 | 32.6 | – | 34.8 | 7 | 1100 |
| 10 QUA | 283.0 | 283 | 281–290 | – | 229.6 | +0.59 | +49.5 | −0.08 | 42.2 | −0.23 | 42.9 | 23 | 3184 |

*Table 3* – Data of the established minor meteor showers sorted by Solar longitude (J2000.0); V and L refer to the values obtained from this video data analysis and taken from the MDC list, respectively. If no activity period is in the list, we type '–' in the respective column. The 32 DLM shower is listed here because of its connection to the 20 COM discussed in the text. $\Delta V_\infty$ is the observed average velocity drift over the activity period in km/s per 1° in Solar longitude. 0 indicates that no drift was observed, while '–' means that no drift can be derived because of too short duration or large scatter of data points.

| Shower | Peak $\lambda_\odot$[°] | | Period $\lambda_\odot$[°] | | Radiant position and drift [°] | | | | $V_\infty$ [km/s] and $\Delta V_\infty$ | | | Max. | Data |
|---|---|---|---|---|---|---|---|---|---|---|---|---|---|
| | (V) | (L) | (V) | (L) | $\alpha$ | $\Delta\alpha$ | $\delta$ | $\Delta\delta$ | (V) | | (L) | VR | Met. |
| 145 ELY | 50 | 49 | 46– 53 | 42– 51 | 291.1 | +0.2 | +43.2 | −0.0 | 43.4 | – | 46.7 | 2.8 | 330 |
| 1 CAP | 125 | 127 | 109–138 | 101–142 | 305.1 | +0.57 | −10.2 | +0.27 | 23.7 | −0.18 | 24.9 | 5.2 | 2283 |
| 191 ERI | 137 | 137 | 132–146 | – | 43.2 | +0.8 | −11.0 | +0.4 | 64.1 | – | 65 | 4.9 | 513 |
| 12 KCG | 141 | 145 | 134–146 | 131–152 | 285.9 | +0.6 | +51.0 | +0.7 | 22.7 | +0.22 | 26.5 | 1.5 | 864 |
| 206 AUR | 158 | 158 | 156–162 | 152–165 | 90.7 | +1.5 | +39.3 | −0.4 | 66.7 | – | 67 | 3.1 | 392 |
| 208 SPE | 167 | 170 | 161–171 | 162–174 | 47.2 | +0.7 | +40.5 | +0.0 | 66.4 | – | 65.5 | 2.6 | 1118 |
| 17 NTA | 231 | 224 | 206–258 | – | 59.7 | +0.84 | +22.7 | +0.15 | 28.5 | −0.09 | 30.4 | 4.1 | 3946 |
| 2 STA | 197 | 224 | 165–237 | – | 31.7 | +0.85 | + 8.7 | +0.18 | 28.9 | −0.05 | 30.4 | 5.7 | 8355 |
| 22 LMI | 210 | 209 | 203–214 | 205–213 | 160.8 | +1.1 | +36.4 | −0.2 | 59.8 | 0 | 62.9 | 4.2 | 550 |
| 18 AND | 230 | 231 | 223–248 | – | 22.8 | +0.2 | +31.4 | +0.86 | 17.8 | 0 | 20.5 | 0.9 | 764 |
| 250 NOO | 248 | 245 | 230–254 | – | 91.9 | +0.73 | +15.2 | −0.03 | 44.1 | −0.22 | 45.1 | 3.2 | 1219 |
| 16 HYD | 254 | 265 | 244–269 | 251–273 | 123.9 | +0.80 | + 2.8 | −0.20 | 60.8 | −0.11 | 59.1 | 4.4 | 1748 |
| 19 MON | 256 | 260 | 255–268 | 245–265 | 99.2 | +0.66 | + 8.1 | −0.15 | 40.9 | 0 | 43.5 | 2.3 | 664 |
| 20 COM | 264 | 268 | 260–271 | – | 174.5 | +0.65 | +18.2 | −0.08 | 67.7 | – | 64.7 | 2.4 | 435 |
| 32 DLM | 268 | 274 | 253–315 | – | 161.5 | +0.86 | +30.5 | −0.43 | 64.0 | 0 | 63.3 | 4.4 | 3181 |
| 319 JLE | 281 | 283 | 280–285 | – | 146.6 | +0.6 | +24.4 | −0.15 | 59.2 | – | 53.9 | 0.6 | 119 |
| 331 AHY | 280 | 286 | 279–289 | – | 125.9 | +0.6 | − 7.9 | −0.14 | 43.4 | – | 45.0 | 1.5 | 187 |

**5 SDA (Southern $\delta$-Aquariids):** this is one of the few strong southern showers with a symmetric maximum (VR = 19 at $\lambda_\odot = 127°$. We find a very long 'tail' of activity, but from 156°(August 30) onwards, the radiant position becomes very uncertain with large scatter. Additionally, VR < 2.0 after $\lambda_\odot = 150°$.

**8 ORI (Orionids):** the surprisingly high peak rate of VR = 68 is mainly caused by the strong returns in the years 2006 to 2008, which make up for more than half of the overall data set. Contrary to the short peak of the Perseids, the Orionid maximum is much wider. As a result, the VR-profile suggests a shower similar in strength to the Perseids. We find VR > 2 already from 183° (September 26), but the radiant position is quite variable until 190° (October 3). At 232° (November 15) we find VR < 2 and again a variable radiant position in consecutive bins (see the remarks earlier in this Section).

**13 LEO (Leonids):** VR > 2 for the entire period, and the radiant deviates from the smooth drift only for the last bin (249°). The varying positions of Leonid peaks and storms over the entire decade cause a relatively wide maximum although each of the individual peaks lasted only for about an hour or so. In total, we can clearly detect Leonids in the period $\lambda_\odot = 223 - 248°$ (November 6–30). We find a further detection in the automatic analysis, yielding a radiant near $\vartheta$ Leonis at $\alpha = 166\,\overset{\circ}{.}0, \delta = 14\,\overset{\circ}{.}4$ with $V_\infty = 71$ km/s at $\lambda_\odot = 253°$ (December 5) which exactly fits the extrapolated Leonid drift. This apparent 'appendix' of the Leonids can be traced over eight bins (251°–258°) with a well detectable VR between 1.3 and 2.8. Perhaps the Leonids extend further than usually expected.

**4 GEM (Geminids):** this strong shower has a rather short activity period with a steep descending branch after the peak at $\lambda_\odot = 261\,\overset{\circ}{.}5$. We find VR ≥ 2.0 for 242–264°, i.e. December 4–16. Two bins at either sides still allow to trace the radiant, but the number of shower meteors becomes very small.

**15 URS (Ursids):** activity is detectable in the interval $\lambda_\odot = 266° - 272°$. Outside this interval, VR is < 0.7 (0.6 in the two preceeding bins, 0.4 in the two consecutive bins). Due to the unique position, the radiant is clear and consistent over the period 266–272°.

**10 QUA (Quadrantids):** we find VR ≥ 0.9 in the entire interval $\lambda_\odot = 274 - 292°$, but similar to the Orionids and as discussed above, the data yield a consistent radiant over the period $\lambda_\odot = 281 - 290°$. The narrow peak occured at slightly different positions over the decade and therefore the high rate occurs in more than one Solar longitude interval (Figure 8). Furthermore, the rate 'tail' after the peak lasts for another four bins to 288° with VR ≥ 2.5 and thus more than three times the detection threshold. Visual data yield ZHR ≥ 5 for 281°–286° and thus also a longer tailing activity than preceeding the maximum (Rendtel & Arlt, 2009; pp. 126–128).

## 6.2 Established minor showers

The analysis should also allow to detect meteor showers of low activity. First, we look at the 'established minor showers'. Of course, the category does not say anything about the strength of the source as compared to the other showers in the MDC list. The automatic analysing procedure indeed provides us with all detectable showers which are in reach of the cameras, although the coverage of the southern hemisphere is much poorer than the northern section. We applied the same limiting factors for the detection as derived from the analysis of the outer regions of the major showers where these essentially are sources of small activity. The results are summarized in Table 3, the activity profiles are shown in Figure 9 and 10. Further, we comment on details of the showers in the text.

**145 ELY ($\eta$-Lyrids):** we find a clearly defined radiant despite the low activity over the period $\lambda_\odot = 46 - 53°$ which is almost exactly coinciding with the entry in the MDC list (see Table 3). The drift of the radiant as found from our data is shown in Figure 11. Our data show a smooth VR-profile (see Figure 9) with a maximum rate of VR = 2.1 at $\lambda_\odot = 50°$. Before 49° and after 52°, the rate is low with values of VR < 1. The agrees well with the activity profile of this shower which was recently included in the IMO's working list (Arlt & Rendtel, 2006).

**1 CAP ($\alpha$-Capricornids):** the radiant of this shower is quite close to the ecliptic and therefore interferes with radiants of the Antihelion Source. The major difference is the velocity which is close to 30 km/s for the Antihelion meteors and 24 km/s for the $\alpha$-Capricornids. The radiant is obvious in the interval between $\lambda_\odot = 109°$ and 138°. Although considered as a minor shower, the activity reaches a maximum VR = 5.2 at $\lambda_\odot = 125°$ and remains above 1.0 for all but the very last bin.

**12 KCG ($\kappa$-Cygnids):** this is another shower with a very low activity. We find VR ≥ 0.8 in the entire period $\lambda_\odot = 135° - 146°$ with a weak maximum of VR = 1.5 at $\lambda_\odot = 141°$ (profile in Figure 9). The radiant is well defined from 134° to 146° with increasing scatter towards the begin and end of the activity period (Figure 12). The entry in the MDC list gives values for the returns in 1993 and 2007 as well as an annual (average?) value. The radiant positions deviate significantly: the 1993 and 2007 radiants are by $5\,\overset{\circ}{.}3$ off in declination alone. Since our data sample includes data of 10 years, a sharp radiant position is not to be expected. Our analysis of short appearances (section 6.5) reveals another radiant at $\alpha = 288\,\overset{\circ}{.}2, \delta = +58\,\overset{\circ}{.}6$ in four bins (149°–152°). The declination fits well with the 2007 data, but the maximum VR is detected only at $\lambda_\odot = 152°$, while the 2007 maximum was observed 11° earlier. This shows that the $\kappa$-Cygnids behave more like a complex than like a single well defined shower.

**206 AUR (Aurigids):** this is the first shower of a series of further sources in the Auriga-Perseus region occurring from end-August to October. This established shower is known for its outbursts. The VR is not high because only the 2007 outburst was recorded by a few

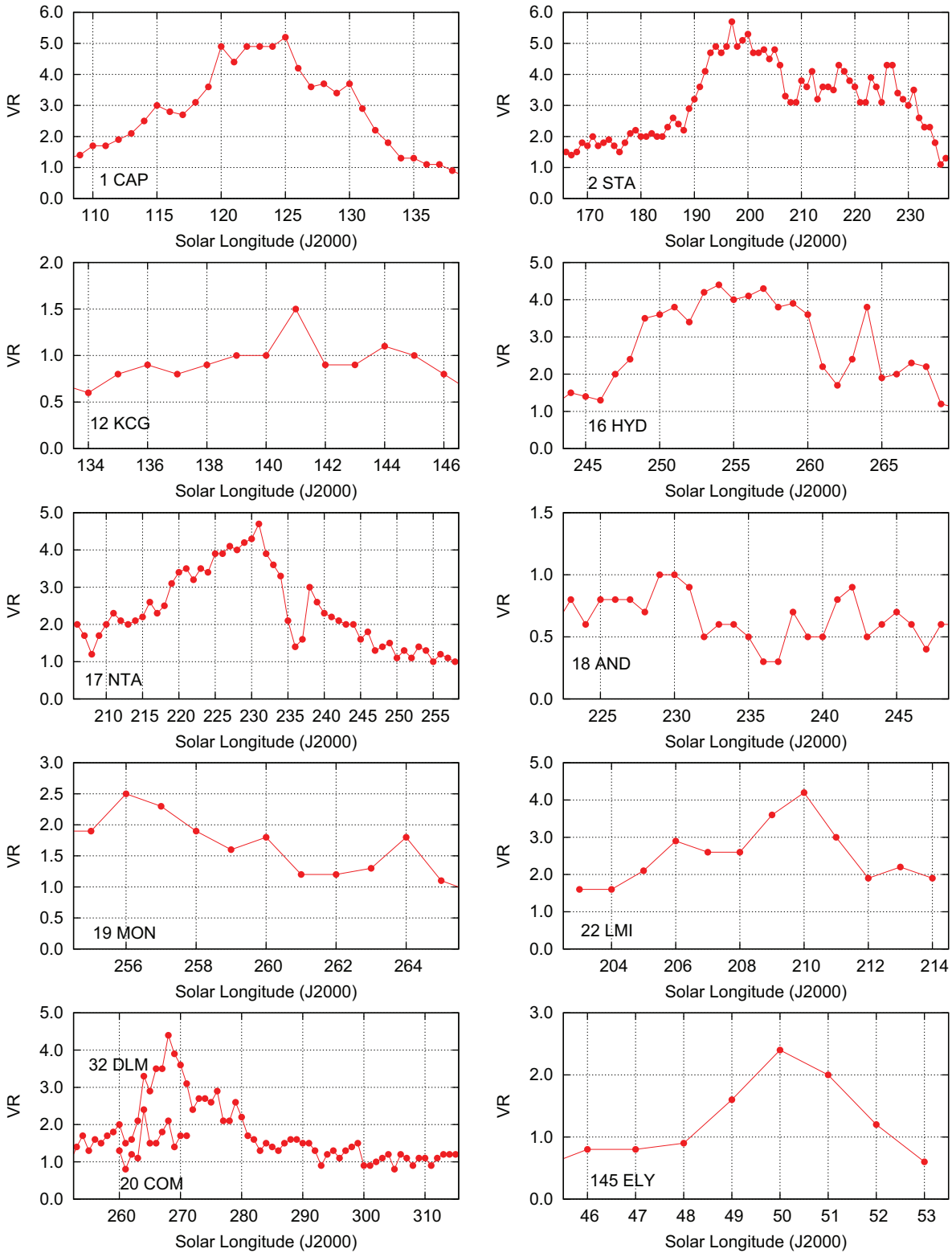


*Figure 9* – Activity profiles for the showers labelled as 'established' in the MDC list derived from our video data, sorted by the MDC shower numbers.

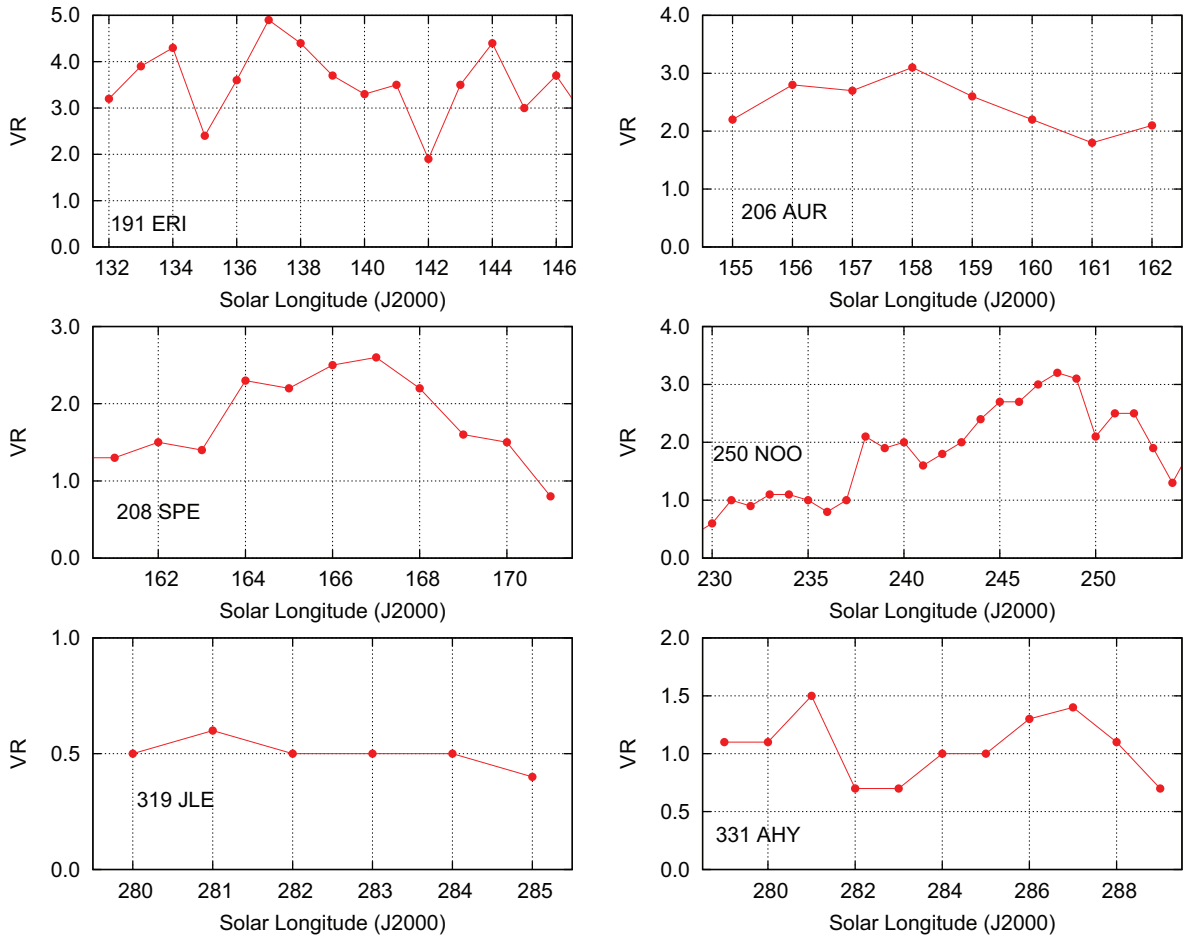


*Figure 10* – Activity profiles for the showers labelled as 'established' in the MDC list derived from our video data sorted by the MDC shower numbers.

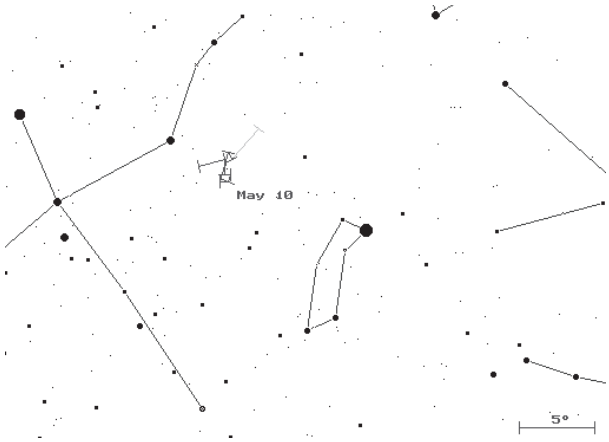


*Figure 11* – Radiant of the $\eta$-Lyrids derived from our video data.

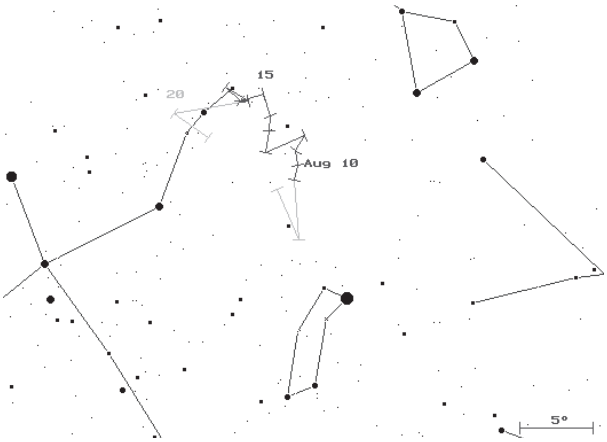


*Figure 12* – Radiant of the $\kappa$-Cygnids derived from our video data.

cameras of the Network. The last one before this happened in 1994.

**208 SPE (September $\varepsilon$-Perseids):** is the second shower of the series mentioned before. The VR reaches 2.6 and remains above 2.0 over five successive bins. It should be emphasized that the radiant obtained from the video data (48 °.0, +39 °.5) differs significantly from the position (60°, +47°) given in the IMO working list (Arlt & Rendtel, 2006). The position listed in the MDC files is 50 °.2, +39 °.4.

**191 ERI ($\eta$-Eridanids):** well detectable activity with a peak VR = 4.9 (Figure 10) and a consistent radiant drift fitting the position given in the list of established showers of the MDC.

**2 STA (Southern Taurids) / 17 NTA (Northern Taurids):** the two branches of the Taurids are

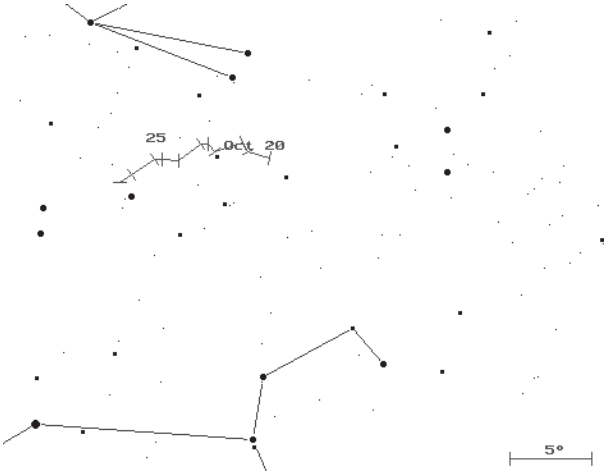


*Figure 13* – Radiant of the Leonis Minorids derived from the video data.

often assumed to coincide in their activity period with weak maxima separated by about two weeks. Our analysis as well as previous studies based on video and visual data show that the situation is somewhat different. The southern branch can be found much earlier, starting at $\lambda_\odot = 165°$ and lasting to 237°; the northern branch can be detected from 206° to 258°. The STA maximum at $\lambda_\odot = 197°$ reaches a VR = 5.7 and is higher than the value of 4.1 found for the NTA at $\lambda_\odot = 231°$. The maxima are thus separated by 34°in Solar longitude. The dip in VR near $\lambda_\odot = 236°$ is not real but an artefact due to the strong Leonid activity at that time.

**22 LMI (Leonis Minorids):** this is another shower which is active during the Orionid period. It produces rates which are clearly above the background. The radiant and activity is well defined from $\lambda_\odot = 203°$ to 214° (Figure 13) and the maximum VR = 4.2 occurs at $\lambda_\odot = 210°$.

**18 AND (Andromedids):** the annual Andromedid shower is a very weak source which can be traced over almost a month. There is no other source interfering with the shower meteor data because of their distinct very low velocity.

**250 NOO (November Orionids)**: only few shower compilations include this weak shower which we can trace from $\lambda_\odot = 233°$ to 254°. It shows a well defined radiant as well as an activity VR $\geq 1.5$ for most of the period (see Figure 10). The highest VR = 3.2 occurs at $\lambda_\odot = 248°$.

**16 HYD ($\sigma$-Hydrids):** this is a minor shower with a reasonably high activity over several bins. We find VR $\geq 4$ in five consecutive bins from 253° to 258° and a maximum VR = 4.7 at $\lambda_\odot = 254°$, also in good agreement with long-term visual results yielding an average maximum ZHR of about 3 (Rendtel & Arlt, 2009). The radiant is well defined from 244° to 269° with a slight deviation against the listed position of $\Delta\alpha = -4°$ and $\Delta\delta = +2°$ at the maximum date. The dip in VR near $\lambda_\odot = 262°$ is not real but an artefact due to the strong Geminid activity at that time.

**19 MON (December Monocerotids):** except the maximum date, all parameters coincide with the listed values. However, the activity is very low and has no pronounced maximum. Our highest VR = 2.5 occurs at 256° and thus 4° earlier than the catalogue date. The radiant can be traced until $\lambda_\odot = 268°$, but the rates are below our threshold in the bins at 266° and 267°.

**319 JLE (January Leonids):** the activity is just below the detection limit and if there were not the entry in the MDC list, we would not have not taken the detection as a signature of a shower. Since its rate remains below the threshold, we do not present an VR-profile here. However, the derived data of the radiant and velocity fit well with the tabulated values.

**331 AHY ($\alpha$-Hydrids):** another established shower with an activity very close to the detection limit. The shower was found automatically from 284° onwards, while the earlier activity was found when we checked for short duration showers. Probably the dominating Quadrantid activity caused that the minor source became undetectable. As in the case of the 319 JLE, the parameters fit well.

**Perseus-Auriga-showers in September and October:** we clearly detect showers in the Perseus-Auriga region from end-August to early October. These include the established shower 206 AUR (Aurigids) and 208 SPE (September $\varepsilon$-Perseids) which have been shortly discussed in the Section 6.2. Further examples are the $\beta$-Aurigids (210 BAU) and the October $\delta$-Aurigids (224 DAU), both having 'working status'. Especially the relation between the 208 SPE and 224 DAU has been analysed in previous papers (Rendtel 1993; Dubietis & Arlt, 2002). However, there is a larger number of showers detectable from this region which requires a more detailed analysis. Therefore we list only the two 'established' sources here.

**20 COM (Comae Berenicids) / 32 DLM (December Leonis Minorids):** this special case needs to be discussed in some detail. The Comae Berenicids (COM) have been in most shower compilations over many years. Recently, an analysis of video data (Molau, 2006) gave no hint at the existence of a radiant at the position listed in the IMO shower list as well as in the MDC list. The same analysis yielded a source which is obviously about 15° west of the radiant given for COM. Our present analysis shows that there are two sources (see the profiles shown in Figure 9). Weak activity from the 'old' radiant listed as Comae Berenicids (20 COM) can be detected in the period 260–271° (December 12–23), but definitively not longer. The other source which was clearly found already in the previous analysis is detectable over a much longer interval 253–315° (December 5 – February 4). The latter produces higher rates – we find a maximum VR = 4.6 at $\lambda_\odot = 268°$. This radiant perfectly fits the position given for the December Leonis Minorids (32 DLM) in the MDC list on December 14 ($\lambda_\odot = 262°$), although our analysis yields the maximum activity on December 20 ($\lambda_\odot = 268°$). The 20 COM is listed as an 'established shower' while the 32 DLM is in the working list.

The question is why this confusing situation occurred. Much of the past information is based on visual data and rather few photographs. Probably, most

of the activity was observed around the Geminid maximum (≈ 262°) and shortly thereafter, i.e. close to 268° (December 20) when both sources are detectable. Meteors occuring later are scarce and in most cases a reliable radiant determination is not possible. Another reason for uncertainties of the radiant position is the distribution of the observed meteors around the radiant. Meteors are observable mostly west and north of the radiant, which is the case especially before local midnight. Hence the position remains unreliable and two possible radiants cannot be distinguished because these are almost on one line. So it could easily be possible that both the existence of two radiants and the ceasing activity from the Comae Berenicids was not correctly observed. The conclusion from our analysis is clear: there are two showers. We find 20 COM for 260–271° (December 12–23) and the other, slightly stronger 32 DLM in the period 253–315° (December 5 – February 4).

## 6.3 MDC showers with working list status

The main achievement of the data set analysed here is the possibility to confirm the existence of showers with MDC working list status and to refine their parameters (radiant position and drift, velocity). Furthermore, we derive information about the video rate VR and thus of the activity period. This was not available for most of the showers compiled in the MDC working list. A summary of our results is listed in Table 4 and the VR-profiles are shown in the Figures 14 and 15. Details for selected cases are described in the text. It must be emphasized that these are all weak sources, often close to the detection limit. As described above, sections of the showers which remain below the thresholds set in the beginning have been omitted. Since the radiant data strongly depend on the number of associated meteors per bin, the drift values remain uncertain in some cases.

**136 SLE ($\sigma$-Leonids):** the radiant is found both in the standard analysis and the manual check for short period meteor activity. Although the VR is just at the detection threshold we listed it here, because the velocity of the meteors is very low and thus the source should be easily distinguishable from the background.

**190 BPE ($\beta$-Perseids):** the data seem to fit the entries in the MDC list quite well. However, the radiant drift is quite uncertain with jumps in consecutive bins. Either the sample is strongly affected by the Perseids with their radiant about 13°north, or the entire radiant is an artefact due to mis-aligned Perseids. Interestingly, the radiant is not found in SonotaCo's list based on orbit determinations.

**23 EGE ($\varepsilon$-Geminids):** this entry of the working list is quite similar to the established $\kappa$-Cygnid shower with low rates and no obvious maximum. The EGE rates are above 2 over the entire activity period. Slightly enhanced rates occur between $\lambda_\odot = 206°$ and 209° (Figure 14), coinciding with the Orionid maximum period. From Figure 16 it is obvious, that the radiant drift is well defined from 203° to 215°.

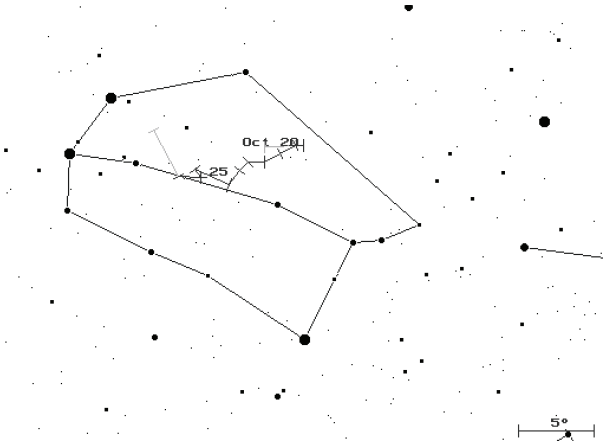


*Figure 16* – Radiant of the $\varepsilon$-Geminids derived from the video data.

**232 BCN (Daytime $\beta$-Cancrids):** interestingly, this shower can be seen in our video data. The right ascension and the velocity fit well with the data of the MDC list, but the declination is by 9° off, probably due to the fact that we can detect only very few meteors in the twilight period appearing to one side of the radiant.

## 6.4 New radiants found from the Network data

Many of the new radiants have been found in the months July and August. This is mainly due to the enormous amount of observational data. Over several years, the collection summarizes a substantial number also from weak sources.

**409 NCY, $\nu$-Cygnids:** this weak source produces a radiant about 30° east of the Lyrids. We carefully checked that these are not Lyrids which are sorted out from the major shower because they may have occurred far away from the radiant. Such meteors could produce a radiant further east with apparently slightly slower meteors. The substantial sample, the consistent radiant data found over the entire period and the large distance to the Lyrids radiant clearly indicate an independent source.

**410 DPI, $\delta$-Piscids:** the video rate VR exceeds 2.5 over the entire detection period, and the radiant drift is well defined. The radiant fits a (backwards) extrapolated drift of the July-Pegasids and the meteors have a similar velocity (67 km/s for JPE, 70 km/s here). However, the shower identified as July-Pegasids (see discussion in section 6.3) is significantly weaker than the source producing this activity. Therefore we propose this as a new radiant rather than the continuation of the July-Pegasids. It might be a similar case as we find it with the series of radiants in the Perseus-Auriga region in September-October.

**411 CAN, c-Andromedids:** the radiant (32°, +49°) is about 30° east of the (extrapolated) Perseid radiant on July 13. At this time, the activity of the Perseids is negligible, so that an interference with erroneously mis-identified and 'shifted' Perseids can be excluded. Of course, the similarity of the velocities (59 km/s) requires caution. The radiant drift shows

*Table 4* – Data of meteor showers included in the MDC working list, sorted by Solar longitude (J2000.0). The MDC list does not give an activity period for the showers of this list – so this is a new information derived from our analysis.

| Shower | Peak $\lambda_\odot$[°] | | Period $\lambda_\odot$[°] | Radiant position and drift [°] | | | | $V_\infty$ [km/s] | | Max. | Data |
|---|---|---|---|---|---|---|---|---|---|---|---|
| | (V) | (L) | (V) | $\alpha$ | $\Delta\alpha$ | $\delta$ | $\Delta\delta$ | (V) | (L) | VR | Met. |
| 40 ZCY $\zeta$-Cygnids | 16 | 20 | 7– 23 | 299.9 | +0.5 | +40.2 | +0.3 | 43.5 | 40.6 | 1.6 | 402 |
| 136 SLE $\sigma$-Leonids | 31 | 28 | 28– 35 | 202.9 | +1.2 | +4.7 | −0.2 | 20.0 | 25.5 | 0.7 | 269 |
| 343 HVI h-Virginids | 32 | 39 | 32– 35 | 214.1 | −1.3 | −11.4 | −1.6 | 24.1 | 21.8 | 1.6 | 192 |
| 175 JPE July Pegasids (*) | 108 | 107 | 105–126 | 347.2 | +0.9 | +11.1 | +0.2 | 68.1 | 62.3 | 1.6 | 591 |
| 184 GDR $\gamma$-Draconids | 125 | 125 | 120–127 | 280.9 | −0.2 | +50.7 | +0.2 | 27.3 | 28.5 | 1.6 | 428 |
| 190 BPE $\beta$-Perseids | 135 | 135 | 132–143 | 44.6 | +0.9 | +40.7 | −0.5 | 67.4 | 67.1 | 2.8 | 1176 |
| 197 AUD Aug. Draconids | 148 | 142 | 138–156 | 275.6 | +0.6 | +62.3 | +0.1 | 23.3 | 20.6 | 1.1 | 951 |
| 337 NUE $\nu$-Eridanids | 164 | 168 | 161–181 | 66.7 | +0.6 | −0.5 | +0.5 | 67.7 | 66.8 | 5.1 | 1185 |
| 234 EPC Oct. $\varepsilon$-Piscids | 196 | 195 | 194–198 | 1.2 | +0.3 | +14.0 | +0.9 | 19.2 | 24.4 | 0.8 | 210 |
| 226 ZTA $\zeta$-Taurids | 203 | 196 | 199–204 | 79.7 | +0.8 | +12.2 | −0.8 | 60.6 | 68.1 | 0.8 | 294 |
| 333 OCU Oct. Ursae Majorids | 202 | 202 | 199–206 | 143.8 | +1.9 | +63.3 | −0.2 | 53.0 | 55.2 | 2.5 | 533 |
| 237 SSA $\sigma$-Arietids | 206 | 202 | 200–210 | 50.7 | +1.1 | +22.1 | 0.0 | 45.5 | 42.0 | 1.0 | 475 |
| 23 EGE $\varepsilon$-Geminids | 206 | 206 | 203–214 | 101.8 | +0.9 | +28.2 | −0.2 | 70.4 | 68.8 | 2.8 | 1134 |
| 241 OUI Oct. Ursae Minorids | 211 | 208 | 206–214 | 273.4 | −1.1 | +74.3 | −0.3 | 27.5 | 32.9 | 0.8 | 308 |
| 232 BCN Dayt. $\beta$-Cancrids | 214 | 213 | 212–221 | 110.5 | +0.8 | −6.1 | +1.2 | 65.1 | 67.0 | 3.4 | 386 |
| 333 OER $o$-Eridanids | 232 | 235 | 231–238 | 60.2 | +0.2 | −1.3 | −0.2 | 27.1 | 29.1 | 1.2 | 229 |
| 339 PSU $\psi$-Ursae Majorids | 253 | 253 | 247–261 | 168.3 | +1.5 | +43.1 | −0.3 | 61.1 | 61.7 | 1.8 | 432 |
| 336 KDR Dec. $\kappa$-Draconids | 251 | 250 | 248–254 | 185.4 | +0.6 | +71.5 | −1.2 | 42.9 | 44.8 | 2.5 | 225 |
| 334 DAD Dec. $\alpha$-Draconids | 253 | 257 | 252–264 | 203.6 | +0.8 | +60.1 | −0.3 | 43.8 | 43.1 | 1.7 | 531 |

(*) JPE: velocity drift observed −0.16 km/s per 1° in Solar longitude

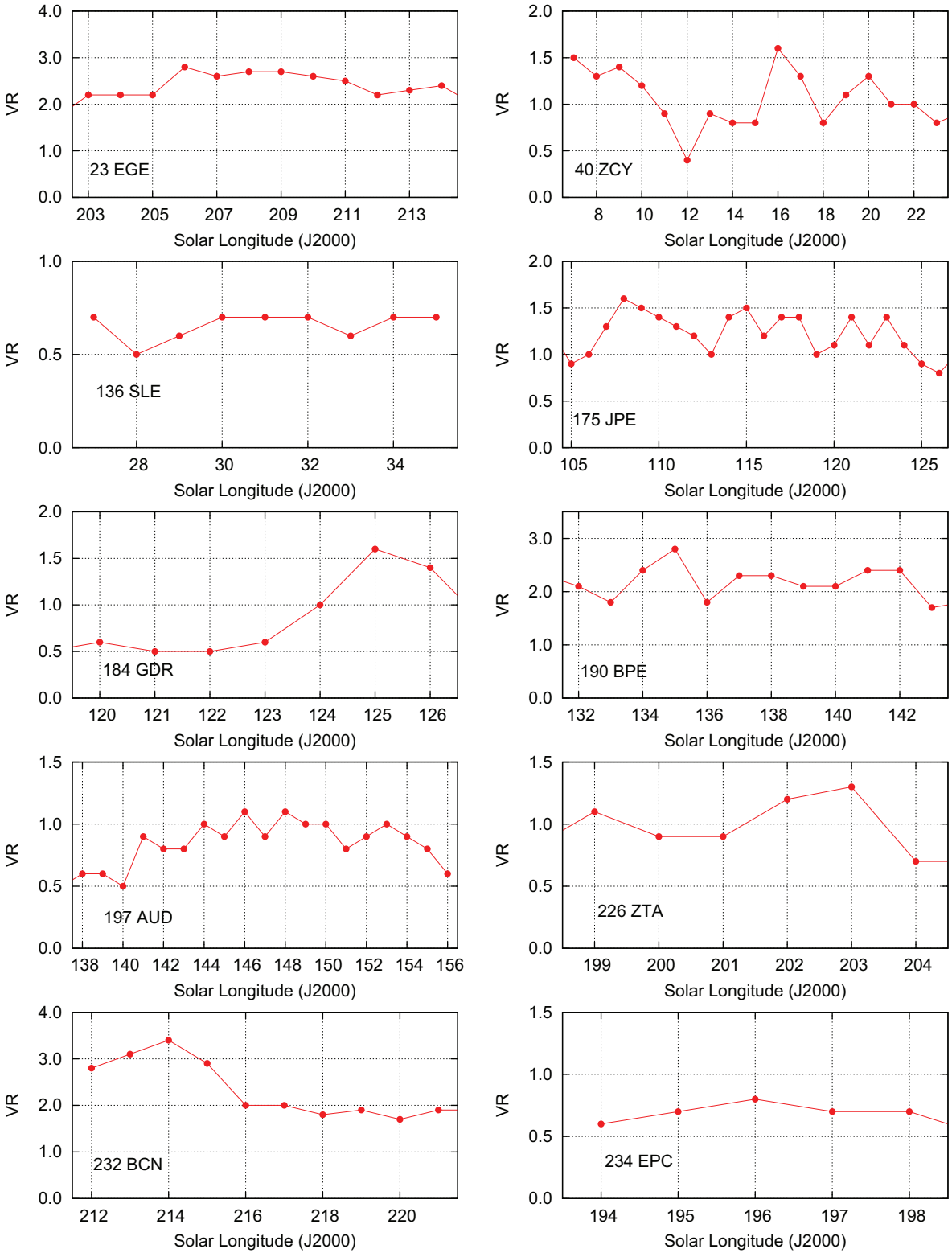


*Figure 14* – Activity profiles for the showers of the 'working list' derived from our video data, sorted by the MDC shower numbers.

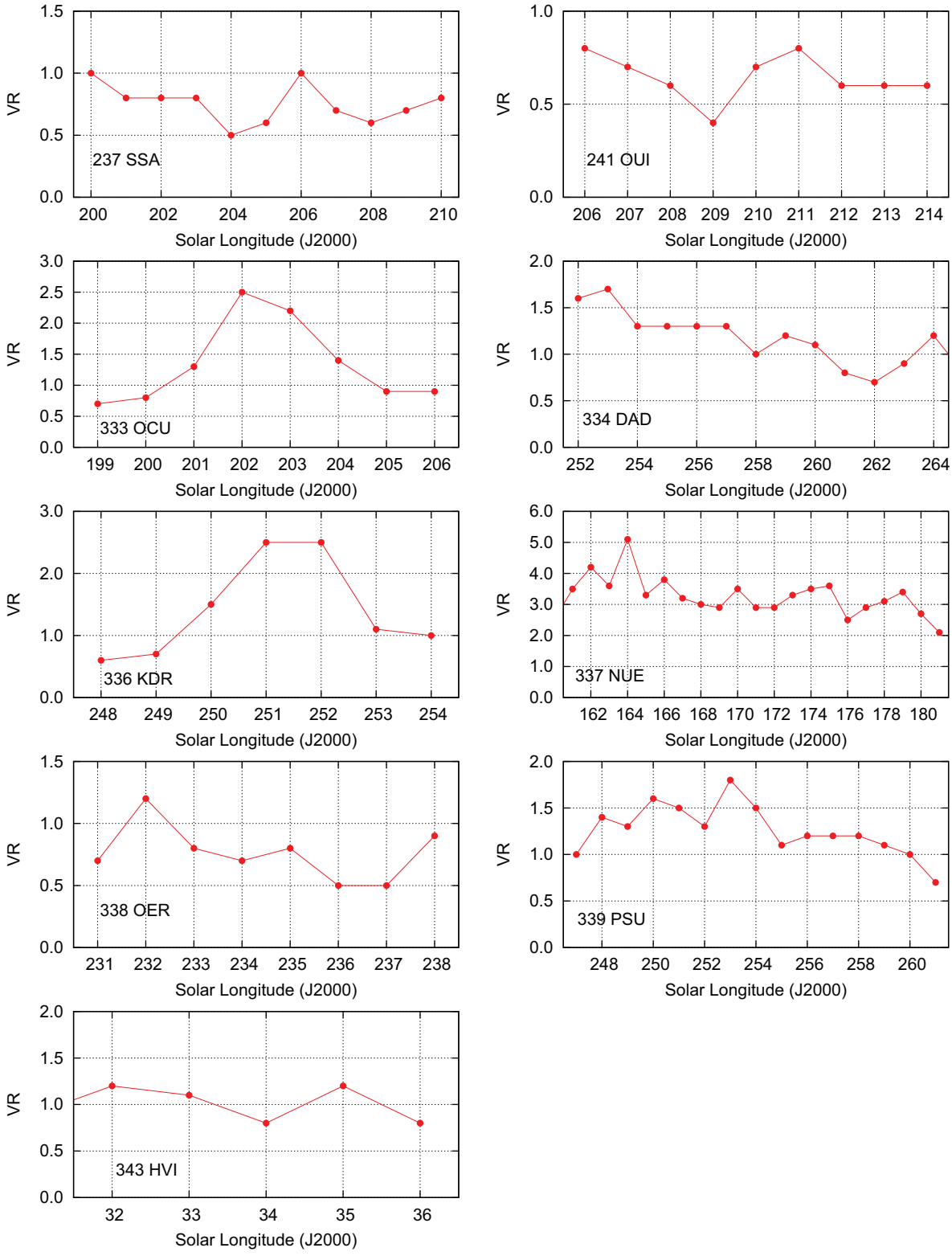


*Figure 15* – Activity profiles for the showers of the 'working list' derived from our video data, sorted by the MDC shower numbers.

*Table 5* – Data of meteor showers found in the IMO Video Meteor Network data, sorted by Solar longitude (J2000.0). The activity data expressed in terms of the video rate (VR) described above is summarized in Figure 17.

| Shower | Max. ($\lambda_\odot$) [°] | Period ($\lambda_\odot$) [°] | Radiant position and drift [°] $\alpha$ | $\Delta\alpha$ | $\delta$ | $\Delta\delta$ | $V_\infty$ [km/s] | VR | Data Met. |
|---|---|---|---|---|---|---|---|---|---|
| 409 NCY $\nu$-Cygnids | 30 | 28– 44 | 305.2 | +1.8 | +39.4 | +0.7 | 42 | 1.8 | 508 |
| 410 DPI $\delta$-Piscids | 92 | 89– 93 | 10.9 | +0.3 | +5.5 | +0.4 | 71 | 4.2 | 105 |
| 411 CAN c-Andromedids | 110 | 102–114 | 32.4 | +1.0 | +48.4 | +0.4 | 59 | 2.3 | 491 |
| 412 FOP f-Ophiuchids | 98 | 96–100 | 266.4 | +4.0 | +8.5 | −0.6 | 21 | 0.7 | 81 |
| 413 MUL $\mu$-Lyrids | 116 | 113–118 | 273.1 | −0.0 | +39.4 | −0.5 | 23 | 0.6 | 129 |
| 414 ATR $\alpha$-Triangulids | 120 | 119–124 | 28.9 | −0.2 | +28.1 | −2.2 | 71 | 3.6 | 192 |
| 73 ZDR $\zeta$-Draconids | 122 | 122–126 | 261.7 | +5.8 | +67.8 | +0.8 | 25 | 0.6 | 148 |
| 415 AUP August Piscids | 132 | 130–137 | 7.5 | +0.9 | +18.3 | +0.1 | 66 | 1.1 | 433 |
| 81 SLY September Lyncids | 167 | 165–172 | 107.4 | +1.7 | +55.0 | +0.3 | 61 | 1.4 | 467 |
| 416 SIC Sep. $\iota$-Cassiopeiids | 169 | 166–171 | 36.7 | −0.2 | +65.0 | +1.0 | 50 | 0.8 | 278 |
| 417 ETT $\eta$-Taurids | 211 | 211–221 | 55.5 | +0.9 | +23.7 | −0.0 | 47 | 1.2 | 323 |
| 418 BHE $\beta$-Herculids | 324 | 322–326 | 246.0 | +0.9 | +23.5 | −0.9 | 55.5 | 1.4 | 99 |

some 'irregular' jumps near $\lambda_\odot = 100 - 102°$ while it is smooth after this date until 114°. The VR varies around 2 with a maximum at $\lambda_\odot = 110°$, i.e. July 13, which coincides approximately with the onset of the 'regular' Perseids. We give 103–114° as the activity period because of the inconsistent early position mentioned above; if this were not the case, we could trace the radiant back to $\lambda_\odot = 96°$.

**412 FOP, f-Ophiuchids:** this source is very weak and thus close to the detection limit. The low velocity of the shower meteors at 21 km/s should remarkably decrease the effect of accidentially aligned sporadic meteors. Particularly at the end of the detection period, after $\lambda_\odot = 104°$, the scatter of the radiant position becomes larger than the limits set for our study. Hence we give an activity period $\lambda_\odot = 99 - 104°$.

**413 MUL, $\mu$-Lyrids:** the radiant at 273°, +39°, could also be named $\vartheta$ Her. This very weak source is another case with a peculiar low $V_\infty = 23$ km/s. As in the case of the f-Ophiuchids, there are no other sources in a wider surrounding region of the sky. The radiant drift is not well defined, but the position is at about 62° ecliptical latitude.

**414 ATR, $\alpha$-Triangulids:** like in September with the Perseus-Auriga showers, there may be more than one source in the vicinity of the (north) apex region in July. The July-Pegasids have been described in the previous section. Meteors from this radiant in Triangulum are found at 71 km/s. An effect from other known sources is not expected because the other radiants are far enough from the radiant.

**73 ZDR, $\zeta$-Draconids:** this radiant is another case formed by slow meteors at 25 km/s coming from almost 70° ecliptical latitude. Like the other two sources with similar low velocity meteors, the video rate VR remains close to the detection limit over the entire period. The drift is not well defined towards the end of the given period. A shower designated as ZDR was already listed in the MDC list. The stored data of radiant position and velocity are based on Lindblad (1971). In this work, two orbits were identified. Similar (slow) meteors give further radiants in Hercules and Cygnus. Jenniskens (2006, p. 712) lists two, the 88 ODR and 182 OCY at 116 and 117°, respectively. The low velocity is common to all these entries. The shower identified from our video data is new and indeed near $\zeta$ Draconis. Hence it was decided in the Task Group on Meteor Shower Nomenclature (Jenniskens et al., 2009), to keep the existing code and to use the new data obtained from this analysis.

**415 AUP, August Piscids:** this source might have some similarity to the $\alpha$-Triangulids discussed before. The radiant is about 15° north of the ecliptic and the velocity of the meteors is rather high (66 km/s). We can trace the radiant for some more days than listed here, but the uncertainties of the position become quite large after $\lambda_\odot = 138°$.

**81 SLY, September Lyncids:** this shower may be associated with others radiating from the Perseus-Auriga region in autumn with similar velocities, such as AUR, SPE or DAU. This radiant is the northernmost found in the region. The radiant can be consistently traced over the entire period from 165° to 172°. Two earlier bins at 162 and 163° also show the radiant with similar strength, but with an uncertain radiant drift. The entry of the 81 SLY also goes back to Lindblad's (1971) paper and the shower data is based on very few graphically reduced photographic orbits. Like in the case of the 73 ZDR, the Task Group proposed to keep the code for the shower but to replace the data with those obtained from our video meteor analysis. Further details are discussed in Section 6.4.

**416 SIC, September $\iota$-Cassiopeids:** we find this shower at $\alpha = 34°, \delta = +65$, with $V_\infty = 50$ km/s in a rather short period around $\lambda_\odot = 169°$. Interferences from other known sources can be excluded.

**417 ETT, $\eta$-Taurids:** in the interval $\lambda_\odot = 211 - 221°$ (Max. 211°), we detect the radiant at $\alpha = 54°, \delta = +24°$; $V_\infty = 47$ km/s, near $\eta$ Tau. Actually, the analysis yields two detections, which obviously define one radiant near the Pleiades with a reliable video rate and a well defined radiant.

**418 BHE, $\beta$-Herculids:** is a shower found from the short activity period check (see Section 6.5). It can be found between $\lambda_\odot = 322$ and 326°. This is a period with a generally low meteor activity and thus suited for the detection of weak sources. The VR of 1.4 is well above the threshold value.

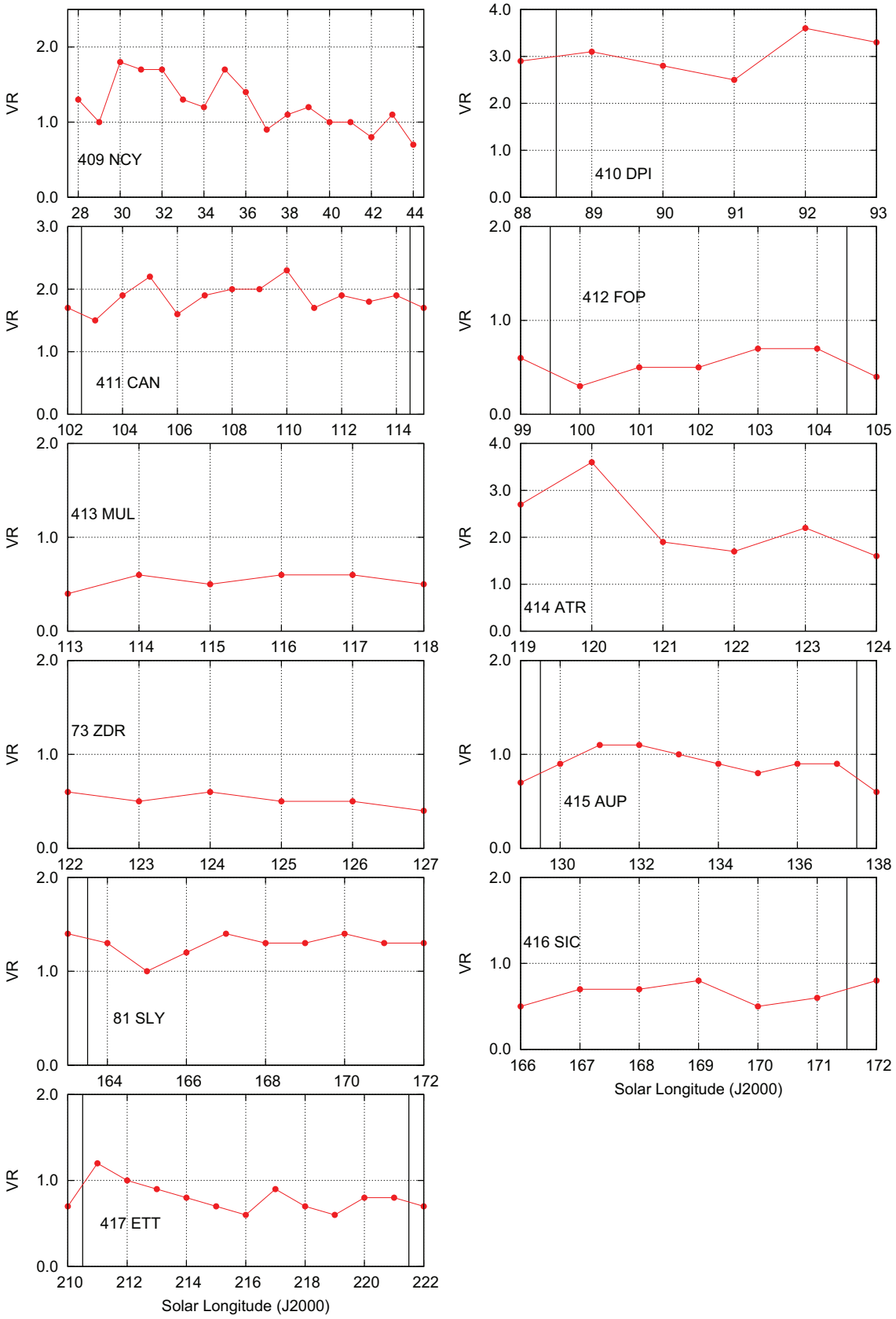


*Figure 17* – Activity profiles of the new showers found from the video data. The vertical lines indicate the limits of the activity period defined by the VR *and* the radiant position. The graphs are sorted as in Table 5.

*Table 6* – Showers of short duration which were detected only in 3–4° intervals of Solar longitude according to the described manual refinement. (V) refers to the results from our video data, (L) to the MDC list.

| Shower | Peak and period $\lambda_\odot$[°] | | | Rad. position, drift (V) [°] | | | | Radiant (L) | | $V_\infty$ [km/s] | | Max. | Data |
|---|---|---|---|---|---|---|---|---|---|---|---|---|---|
| | (V) | (L) | (V) | $\alpha$ | $\Delta\alpha$ | $\delta$ | $\Delta\delta$ | $\alpha$ | $\delta$ | (V) | (L) | VR | Met. |
| 43 ZSE $\zeta$-Serpentids | 4 | 365 | 3– 7 | 256.2 | +2.1 | −4.1 | +0.4 | 266.3 | −6.3 | 63.8 | 68.4 | 1.5 | 86 |
| 136 SLE $\sigma$-Leonids | 23 | 28 | 21– 24 | 199.5 | −0.5 | +3.6 | −0.6 | 192.6 | +3.1 | 22.7 | 25.6 | 1.1 | 129 |
| 149 NOP N. May Ophiuchids | 52 | 50 | 47– 53 | 237.1 | +1.6 | −8.2 | +0.9 | 249.0 | −14.0 | 28.0 | 30.0 | 1.8 | 291 |
| 337 NUE $\nu$-Eridanids | 165 | 168 | 162–165 | 74.7 | +0.6 | +0.3 | −1.9 | 68.7 | +1.1 | 67.0 | 66.8 | 3.7 | 157 |
| 81 SLY Sept. Lyncids | 186 | 185 | 186–189 | 110.2 | −2.9 | +48.4 | −0.7 | 110.0 | +47.9 | 67.7 | 66 | 1.6 | 237 |
| 323 XCB $\xi$-Coronae Borealids | 295 | 295 | 290–295 | 248.3 | −0.2 | +29.2 | −0.1 | 244.8 | +31.1 | 50.1 | 45.7 | 1.2 | 105 |
| 97 SCC South. $\delta$-Cancrids | 298 | 296 | 294–298 | 131.5 | +1.7 | +10.6 | −1.0 | 134.1 | +10.1 | 28.7 | 27.6 | 0.9 | 134 |
| 101 PIH $\pi$-Hydrids | 319 | 317 | 315–319 | 215.2 | +1.0 | −26.2 | −1.9 | 210.3 | −23.0 | 69.7 | 71.6 | 3.2 | 88 |

### 6.5 Short duration showers

The standard procedure as decribed above requires a radiant to be detected over five degrees in Solar longitude. Consequently, it omits short duration showers, such as the Draconids. In order to find active sources which are detectable over a shorter period of time, we run an additional analysis allowing for a minimum of three degrees length only. Of course, many known sources re-appeared and several unreliable sources showed up, which is why we concentrated only on strong sources or those fitting to showers from the MDC list. Overall, nine additional sources have been detected, among these one new source, named 418 BHE ($\beta$-Herculids; see Section 6.4). The results from the short interval analysis are summarized in Table 6.

The procedure finds radiants which fit the data of the Northern May Ophiuchids (149 NOP) reasonably well in two separate intervals. Both radiants differ from the listed position, and the velocity fits better in the second period ($\lambda_\odot = 47° - 53°$) which is included in Table 6.

81 SLY is found not only in the short interval listed in Table 6 but was detected automatically by the standard procedure. This procedure reveals the SLY in two periods (179°–184° and 189°-194°) with an interruption in the center. The radiant is close to the apex, which is also detected as a relatively strong source in this interval. Hence we expect an interference from apex meteors leading to an uncertain radiant position of the weak September Lyncids. Consequently, we list the shower only in the central short interval in which the fit with the listed data is best and VR = 1.6. A recent discussion in the Task Group (Jenniskens, 2009) as well as the analysis of our data set yielded a likely connection between the 81 SLY as they were included in the existing MDC list on the one hand and our new detection (now the 81 SLY as described in the Section 6.4 and Table 5) and the short-duration activity discussed here on the other hand. However, the fact that our analysis yielded two detections (the 'new' radiant and the slightly deviating short duration shower) indicates, that the case is not yet completely solved. At the moment, we cannot match all detections to describe one continuous source. We either see one source at different activity intervals or more than one shower (with similar physical data) being part of the already mentioned complex in the Perseus-Auriga region. Details will be presented in the respective upcoming analysis.

### 6.6 Established showers from the MDC list not found in our data

Many, but not all showers that are marked as established in the MDC list were found in our analysis. There are several reasons why a shower may have been missed.

(i) The shower is too weak or occurs at a time of year that is poorly covered by observations. Chances for this are low, because our total sample has a good coverage of the entire year.

(ii) The activity interval of the shower is too short, or the shower is not permanently active: We will have missed showers, which show only once in a few years significant activity or who are active for only one or two days. AMO and JBO are such showers.

(iii) The radiant lies far south. Most meteor observations were obtained from the northern hemisphere. There is also a subset of about 15 000 meteors recorded from Australia, but in general the coverage of the southern hemisphere is poor. The geographical distribution of the cameras should allow to detect all significant meteor showers north of $\delta \approx -25°$. 'Established' showers south of this limit are ACE, BHY, GNO, PHO, PUP, and PPU.

(iv) The meteors are too faint to be detected by video. If meteor showers were detected by radar, they might be composed of meteors beyond the limit of video observation.

(v) The meteors occur at daytime. Most daytime meteor showers cannot be detected in the optical domain.

Several established MDC list showers were missing in our analysis. So we checked the original radiant set of the analysis per Solar longitude bin whether we find traces of these showers.

**102 ACE ($\alpha$-Centaurids):** no traces of this far southern radiant, but our sample includes only few respective data.

**11 EVI ($\eta$-Virginids):** radiant is clearly visible in our data. As it is close to the antihelion source, we have not listed this shower separately here. Another shower, 123 NVI (Northern March Viginids), has essentially the same position but a lower velocity. Our data fits the 11 EVI.

**27 KSE ($\kappa$-Serpentids):** in the interval 14–16° we find weak radiants which could fit the KSE data. $\lambda_\odot$=14°: 230.°5, +12.°5, 43 km/s; $\lambda_\odot$=15°: 227.°4, +12.°5, 45 km/s; $\lambda_\odot$=16°: 221.°8, +17.°5, 47 km/s.

**21 AVB ($\alpha$-Virginids):** in our analysis we find one weak detection in the region which does not fit well. It is located at 197°, −6.°5, $V_\infty$=20 km/s at 29° Solar longitude.

**137 PPU ($\pi$-Puppids):** not found in our analysis due to its southern position and the low activity except its outbursts.

**55 ASC ($\alpha$-Scorpiids:)** this is another radiant which is near the Antihelion source. Our analysis yields two detections at 54° and 55° which are more than 10° northeast at 256°, −23.°5 and correspond to $V_\infty$ = 37 km/s.

**61 TAH ($\tau$-Herculids):** no signs in our analysis.

**165 SZC (Southern June Aquilids):** could be a very short duration shower. At $\lambda_\odot = 79°$ find a radiant at 302.°8, −33.°5, $V_\infty$ = 35.0 km/s which fits the listed values reasonably. The next two bins also show a radiant close to the position (304°, −34°) but composed of meteors with 45 km/s.

**164 NZC (Northern June Aquilids):** can be detected in our results, although the routine matched our data with the 179 SCA ($\sigma$-Capriconids). Both are not too far from the Antihelion source.

**63 COR (Corvids):** $V_\infty = 14.4\,\mathrm{km/s}$ – meteors at such very low velocities should be easily distinguished from the background, but the analysis yields no sign of this shower. During the observed years there was obviously no activity present.

**170 JBO (June Bootids):** is found only as an extremely weak detection at $\lambda_\odot = 97°$ ($229\overset{\circ}{.}5, +43\overset{\circ}{.}5$, $V_\infty = 18.0$ km/s). As found in other analyses, the activity is essentially zero outside the outburst intervals.

**187 PCA ($\psi$-Cassiopeiids):** despite the position far from other sources and not interfering with activity periods of other showers, nothing is found in our data.

**183 PAU (Piscis Austrinids):** we find weak signs earlier between 113 and 117°, but the data remained below our thresholds for shower detection.

**3 SIA (Southern $\iota$-Aquariids):** is difficult to separate from the strong 5 SDA. The analysis gives radiants in the vicinity of the SDA over the activity period, espcially at 127° and 130°, but no consistent radiant which could be identified as SIA.

**198 BHY ($\beta$-Hydrusids):** lacks from the small amount of data for this far southern radiant.

**233 OCC (October Capricornids):** nothing is found in our data.

**281 OCT (October Camelopardalids):** radiant $\alpha = 168\overset{\circ}{.}3, \delta = +78\overset{\circ}{.}0, V_\infty = 44.5\,\mathrm{km/s}$ at $\lambda_\odot = 192.9°$ is clearly visible between 192 and 193°, but not found by the automatic procedure because of the very short activity interval. The maximum video rate is VR = 2.0 and thus above the thresholds (based on 118 meteors).

**9 DRA (October Draconids):** the radiant $\alpha = 262°, +56°, V_\infty = 19$ km/s at $\lambda_\odot = 195\overset{\circ}{.}5$ is detected between 195 and 196°, but the duration is too short for the automatic procedure. The maximum video rate is VR = 0.8 (only 80 meteors as the sample does not include any period of enhanced activity).

**246 AMO ($\alpha$-Monocerotids):** this is an established shower which cannot be found in our analysis. It is famous for its short-lived outbursts of which the last was observed in 1995. In all other years, the rates remained close to the detection limit. Our data show signs of a very weak AMO activity. However, the radiant deviates from the outburst position in right ascension and declination. Actually, the analysing procedure yields two radiants on both sides of the known position with the more northern one producing a higher rate (maximum VR = 2.7 at 238°). Furthermore, we find the best fitting velocity deviates by −3 km/s for the radiant south of the listed position, but +4 km/s for the radiant north of the listed position. This indicates some artefacts, possibly due to uneven distribution of associated shower meteors around the radiant position.

**254 PHO (Phoenicids):** lacks from the small amount of data for this southern radiant.

**256 ORN (Northern $\chi$-Orionids:** is part of the Antihelion source and continues the Southern Taurid activity. The analysis detects the radiant, but we do not analyse it here separately.

Not unexpectedly, the daytime (D.) showers 141 DCP (D. $\chi$-Piscids), 144 APS (D. April Piscids), 153 OCE (Southern D. $\omega$-Cetids), 171 ARI (D. Arietids), 172 ZPE (D. $\zeta$-Perseids), 173 BTA (D. $\beta$-Taurids), 188 XRI (D. $\xi$-Orionids) and 221 DSX (D. Sexantids) did not occur in our analysis.

## 7 Summary and Conclusions

As summary, we show two figures that present all meteor shower radiants detected in the IMO Video Meteor Database in a sinusoidal projection with right ascension on the abscissa and declination on the ordinate (Figure 18). The meteor shower velocity is color coded. It is worth to compare the plot with the presentation of the Japanese results in SonotaCo (2009), Figure 5 and back cover of the respective WGN issue. All significant features are found in both plots. Note, however, that the plots are created in slightly different ways. From double-station data like the SonotaCo analysis, a unique radiant point (right acsencion, declination, velocity) is obtained for each individual meteor recorded by two or more stations. Hence, each dot represents a single meteor in their graph. From single station data as presented here, the radiant position is ambiguous: For each meteor, there are several possible radiant points with different positions and velocities along the backward trace. Only when large data sets are analysed in a statistical way, we find radiant points composed by several meteors. These radiant points are depicted in Figure 18, i.e. here each dot represents approximately 50 single station meteors on average, with a range between 10 and 10 000. Meteor showers show up as cluster of points in the SonotaCo plot, but they would get lost in our graph because even thousands of meteors are represented by a single dot. For this reason, we coded the meteor number with the brightness: the brighter a dot, the more meteors contributed to the radiant.

Figure 19 is our version of the corresponding Figure 6 in the SonotaCo paper. Here, the abscissa represents the difference between the ecliptical radiant longitude and the solar longitude, and the ordinate the ecliptical latitude of the radiant. The similarity of both plots is amazing and underlines the abilities of the method presented here.

Recent radiant searches (SonotaCo, 2009; Brown et al., 2008, 2009) gave not only new positions of shower radiants but increased also our knowledge about the physical parameters and the extensions of the streams. The list of nine major and 44 minor showers analysed here show that the procedures work well. Cross-comparisons also demonstrate that the results obtained from independent data sets and applying different methods reveal consistent and therefore reliable results. Hence the detection of twelve new showers is not surprising. Further, the shift in velocity over the activity period found here and confirmed for several examples from SonotaCo's independent data sample demonstrates that the continuous collection of data is not only useful for an increasing accuracy of existing data but also for new results.

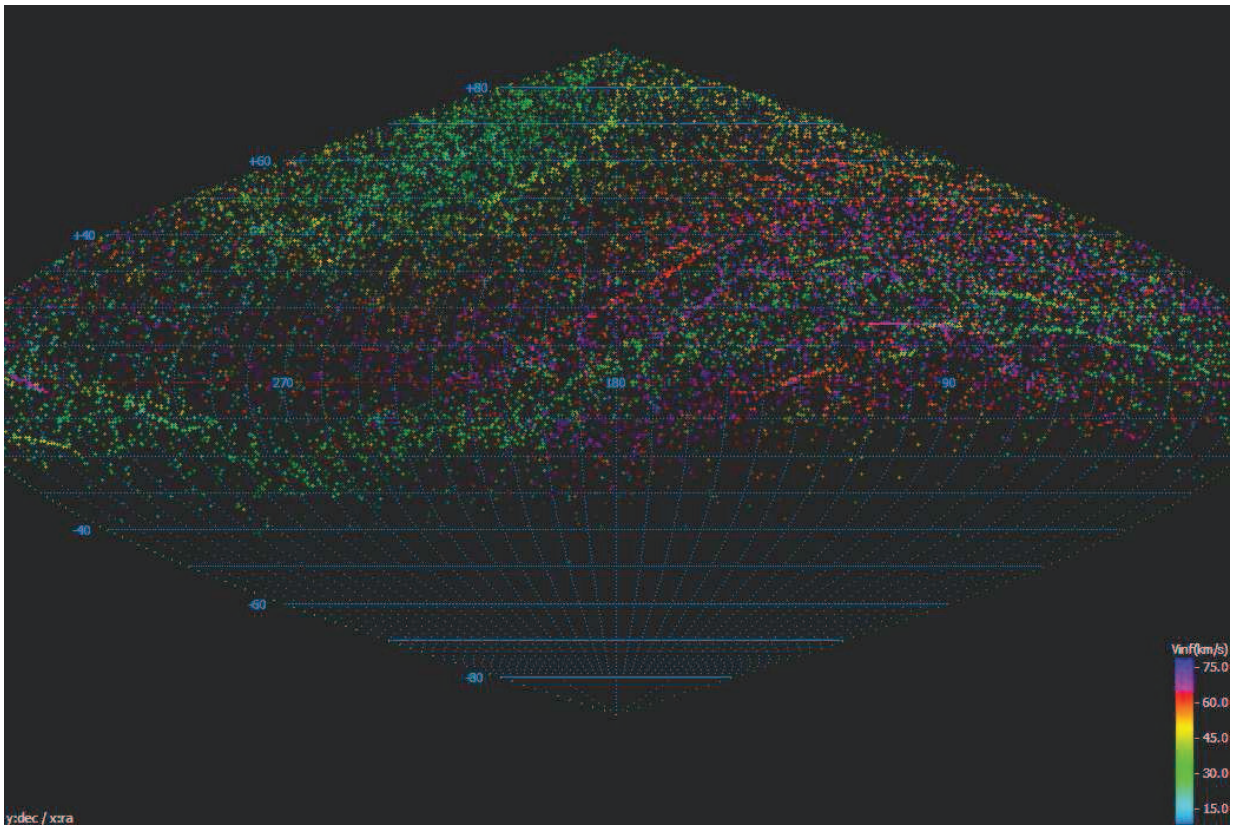


*Figure 18* – Distribution of radiants detected in the IMO Video Meteor Database over right ascension and declination in a sinusoidal projection. The brightness of each spot represents the number of meteors that contributed to the radiant, and the meteor shower velocity is coded in the color (reproduced on the back cover).

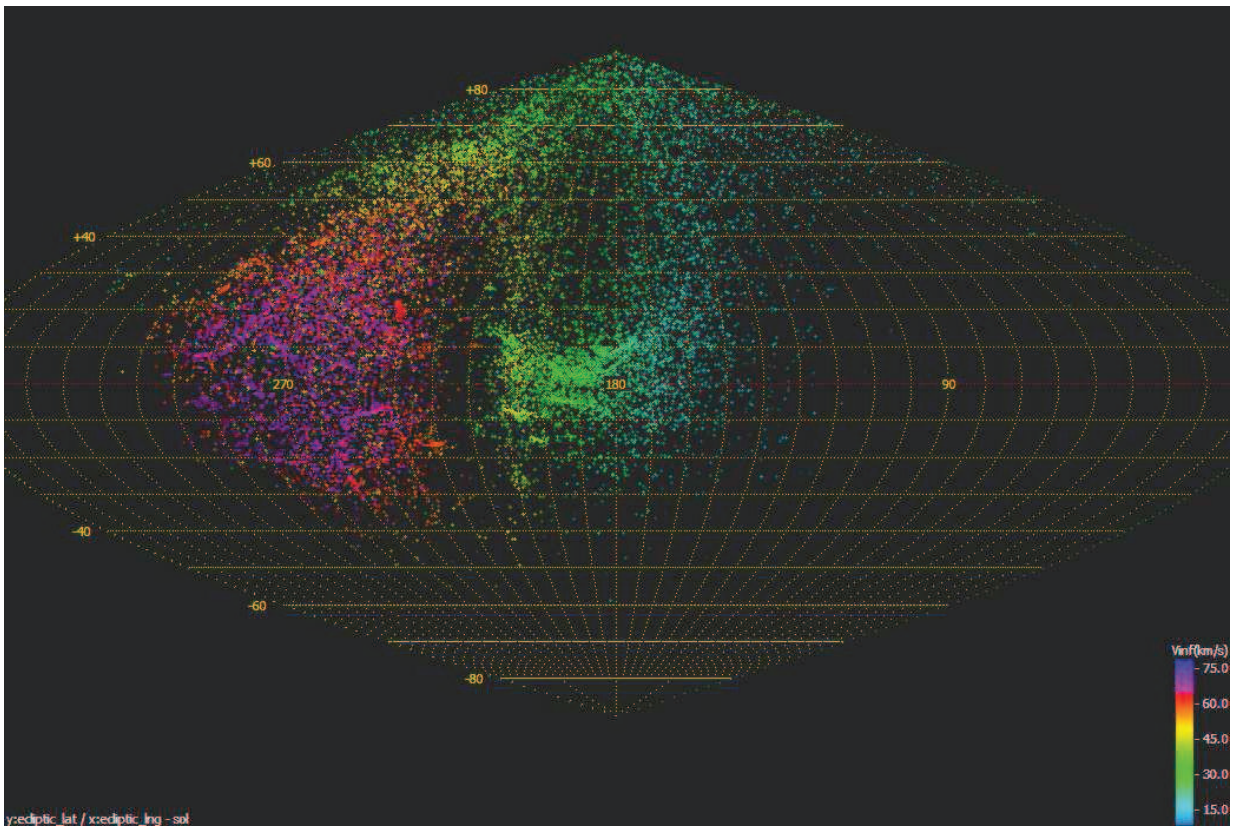


*Figure 19* – Distribution of radiants detected in the IMO Video Meteor Database in Sun-centered ecliptical coordinates with the ecliptical radiant longitude minus the solar longitude as x-axis, and the ecliptical latitude as y-axis.

## 8 Acknowledgements:

We are in debt of all video camera operators (see Table 1) who provide us with their meteor data on a regular basis and lay the foundation for analyses like this. Even if the observation is largely automated these days, it still requires a lot of passion and patience to set up a video system, get used to the analysis software, operate one or even multiple cameras for several years and process the data before they are collected in the central database.

In particular, we like to thank the Japanese meteor observer, UFO* programmer and meteor network operator SonotaCo. In recent years, we could establish vivid contacts between the networks and learn a lot from each other and together in cooperation. The SonotaCo network provides us with the unique chance to check our findings with an independent dataset, just as we can provide further evidence to findings of the SonotaCo network. For this paper, SonotaCo provided us with the radiant plots (Figure 18 and 19). He confirmed the variation of meteor shower velocities that we detected, and provided fruitful discussions and valuable input for the meteor shower lists.

## References

Arlt R. and Rendtel J. (2006). "A new working list of meteor showers". *WGN, Journal of the IMO*, **36**, 77–84.

Brown P., Weryk R. J., Wong D. K., and Jones J. (2008). "A meteoroid stream survey using the Canadian meteor orbit radar I: Methodology and radiant catalogue". *Icarus*, **195**, 317–339.

Brown P., Wong D. K., Weryk R. J., and Wiegert P. (2009). "A meteoroid stream survey using the Canadian meteor orbit radar II: Identification of minor showers using a 3D wavelet transform". *Icarus*. (submitted).

Dubietis A. and Arlt R. (2002). "The current Delta-Aurigid meteor shower". *WGN, Journal of the IMO*, **30**, 168–174.

Jenniskens P. (2006). *Meteor showers and their parent comets*. Cambridge Univ. Press.

Jenniskens P., Jopek T. J., Rendtel J., Porubčan V., P. P. S., Baggaley J., Abe S., and Hawkes R. (2009). "On how to report new meteor showers". *WGN, Journal of the IMO*, **37**, 19–20.

Jopek T. J. (2009). "IAU Meteor Data Center". `http://www.astro.amu.edu.pl/~jopek/MDC2007` .

Lindblad B. A. (1971). "A computerized stream search among 2401 photographic meteor orbits". *Smithosn. Contr. Astrophys.*, **12**, 14–24.

Molau S. (1998). "The meteor detection software MetRec". In Arlt R., editor, *Proc. IMC 1998, Stara Lesná, Slovakia*, pages 9–16. International Meteor Organization.

Molau S. (2001). "The AKM Video Meteor Network". In Warmbein B., editor, *Proc. Meteoroids 2001, Kiruna, Sweden*, pages 315–318.

Molau S. (2006). "How good is the IMO Working List of meteor showers? A complete analysis of the IMO video meteor database". In Bettonvil F. and Kac J., editors, *Proc. IMC 2006, Roden, the Netherlands*, pages 38–54.

Molau S. (2008). "A new analysis of the IMO video meteor database". In *Proc. IMC 2008, Šachticka, Slovakia*.

Molau S. and Kac J. (2009). "Results of the IMO video meteor network – December 2008". *WGN, Journal of the IMO*, **37**, 43–47.

Molau S. and SonotaCo (2008). "On the average altitude of (video) meteors". *WGN, Journal of the IMO*, **36**, 124–130.

Rendtel J. (1993). "Radiants and orbits of $\delta$-Aurigids and September Perseids". In *Proceedings of the IMC Smolenice 1992*, pages 67–73.

Rendtel J. and Arlt R., editors (2009). *Handbook for meteor observers*. International Meteor Organization.

SonotaCo (2009). "A meteor shower catalog based on video observations in 2007–2008". *WGN, Journal of the IMO*, **37**, 55–62.

*Handling Editor:* Javor Kac

This paper has been typeset from a LaTeX file prepared by the authors.